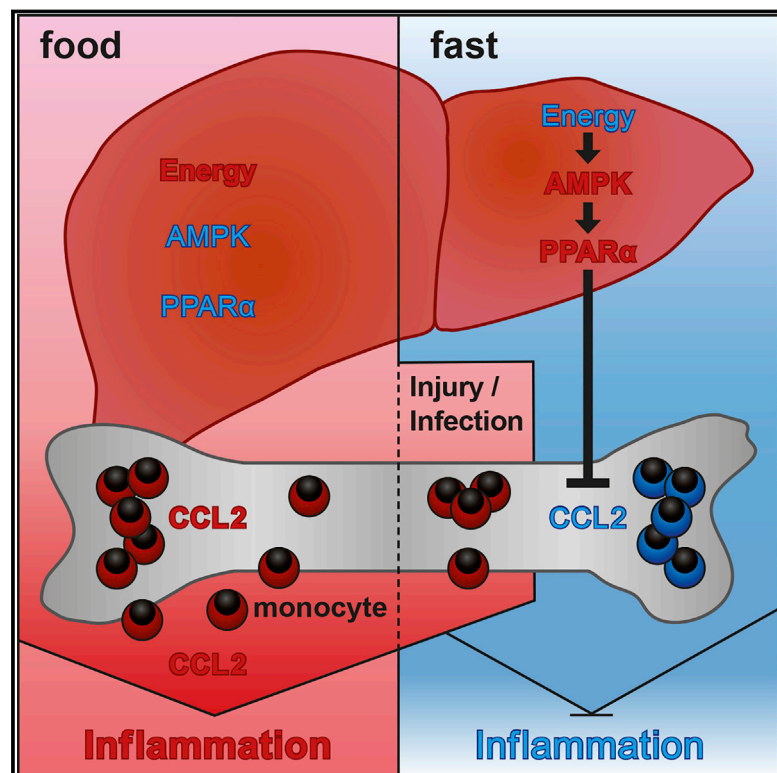


Dietary Intake Regulates the Circulating Inflammatory Monocyte Pool

Graphical Abstract



Authors

Stefan Jordan, Navpreet Tung, Maria Casanova-Acebes, ..., Marie-Luise Berres, Emily J. Gallagher, Miriam Merad

Correspondence

miriam.merad@mssm.edu (M.M.), stefan.jordan@mssm.edu (S.J.)

In Brief

Caloric restriction reduces the number of circulating inflammatory monocytes in a CCL2/PPAR α -dependent manner, without compromising responses to acute inflammation.

Highlights

- Fasting reduces the numbers of circulating monocytes in healthy humans and mice
- Fasting also reduces monocyte metabolic and inflammatory activity
- Hepatic energy-sensing regulates homeostatic monocyte numbers via CCL2 production
- Fasting improves inflammatory diseases without compromising antimicrobial immunity



Dietary Intake Regulates the Circulating Inflammatory Monocyte Pool

Stefan Jordan,^{1,2,3,*} Navpreet Tung,^{1,2,3} Maria Casanova-Acebes,^{1,2,3} Christie Chang,^{1,2,3} Claudia Cantoni,¹³ Dachuan Zhang,⁸ Theresa H. Wirtz,⁹ Shruti Naik,¹⁰ Samuel A. Rose,⁴ Chad N. Brocker,¹¹ Anastasiia Gainullina,^{12,14} Daniel Hornburg,¹⁵ Sam Horng,⁶ Barbara B. Maier,^{1,2,3} Paolo Cravedi,² Derek LeRoith,⁵ Frank J. Gonzalez,¹¹ Felix Meissner,¹⁵ Jordi Ochando,¹ Adeeb Rahman,^{3,4,7} Jerry E. Chipuk,^{1,3} Maxim N. Artyomov,¹² Paul S. Frenette,⁸ Laura Piccio,^{13,16} Marie-Luise Berres,⁹ Emily J. Gallagher,⁵ and Miriam Merad^{1,2,3,17,*}

¹Department of Oncological Sciences, Icahn School of Medicine at Mount Sinai, 1 Gustave L. Levy Place, New York, NY 10029, USA

²The Precision Immunology Institute, Icahn School of Medicine at Mount Sinai, 1 Gustave L. Levy Place, New York, NY 10029, USA

³The Tisch Cancer Institute, Icahn School of Medicine at Mount Sinai, 1 Gustave L. Levy Place, New York, NY 10029, USA

⁴Department of Genetics and Genomic Sciences, Icahn School of Medicine at Mount Sinai, 1 Gustave L. Levy Place, New York, NY 10029, USA

⁵Division of Endocrinology, Diabetes and Bone Diseases, Icahn School of Medicine at Mount Sinai, 1 Gustave L. Levy Place, New York, NY 10029, USA

⁶Department of Neurology and Neuroscience, Icahn School of Medicine at Mount Sinai, 1 Gustave L. Levy Place, New York, NY 10029, USA

⁷Human Immune Monitoring Center, Icahn School of Medicine at Mount Sinai, 1 Gustave L. Levy Place, New York, NY 10029, USA

⁸Ruth L. and David S. Gottesman Institute for Stem Cell and Regenerative Medicine Research, Department of Cell Biology, Albert Einstein College of Medicine, 1301 Morris Park Avenue, The Bronx, NY 10461, USA

⁹Department of Internal Medicine III, University Hospital, RWTH Aachen, Pauwelsstrasse 30, 52074 Aachen, Germany

¹⁰Department of Pathology, and Ronald O. Perleman Department of Dermatology, NYU School of Medicine, 240 East 38th Street, New York, NY 10016, USA

¹¹Laboratory of Metabolism, Center for Cancer Research, National Cancer Institute, National Institutes of Health, Building 37, Bethesda, MD 20892, USA

¹²Department of Pathology & Immunology, Washington University School of Medicine, 660 South Euclid Avenue, St. Louis, MO 63110, USA

¹³Department of Neurology, Washington University School of Medicine, 660 S Euclid Avenue, St. Louis, MO 63110, USA

¹⁴Computer Technologies Department, ITMO University, Kronverksky 49, Saint Petersburg, Russian Federation

¹⁵Max-Planck-Institute of Biochemistry, Am Klopferspitz 18, 82152 Martinsried, Germany

¹⁶Brain and Mind Centre, University of Sydney, 94 Mallett Street, Camperdown NSW 2050, Australia

¹⁷Lead contact

*Correspondence: miriam.merad@mssm.edu (M.M.), stefan.jordan@mssm.edu (S.J.)

<https://doi.org/10.1016/j.cell.2019.07.050>

SUMMARY

Caloric restriction is known to improve inflammatory and autoimmune diseases. However, the mechanisms by which reduced caloric intake modulates inflammation are poorly understood. Here we show that short-term fasting reduced monocyte metabolic and inflammatory activity and drastically reduced the number of circulating monocytes. Regulation of peripheral monocyte numbers was dependent on dietary glucose and protein levels. Specifically, we found that activation of the low-energy sensor 5'-AMP-activated protein kinase (AMPK) in hepatocytes and suppression of systemic CCL2 production by peroxisome proliferator-activator receptor alpha (PPAR α) reduced monocyte mobilization from the bone marrow. Importantly, we show that fasting improves chronic inflammatory diseases without compromising monocyte emergency mobilization during acute infectious inflammation and tissue repair. These results reveal that caloric intake and liver energy sensors dictate the blood and tissue im-

une tone and link dietary habits to inflammatory disease outcome.

INTRODUCTION

Caloric excess, frequent in the Western world, has been linked to systemic low-grade chronic inflammation (Lumeng and Saltiel, 2011) and is thought to contribute to numerous diseases including metabolic syndrome (MetS), non-alcoholic fatty liver diseases (NAFLD), type 2 diabetes mellitus (T2DM), atherosclerosis, cardiovascular disease (CVD), and other related co-morbidities (Haslam and James, 2005). Accordingly, the recent diet westernization of developing countries has been associated with an increased prevalence of inflammatory or autoimmune disorders (Manzel et al., 2014). In contrast, hypocaloric diets or fasting regimens are associated with improved outcomes of metabolic, autoimmune, and inflammatory diseases in humans, including NAFLD (Kani et al., 2017), T2DM (Zubrzycki et al., 2018), CVD (Wei et al., 2017), multiple sclerosis (Choi et al., 2016), rheumatoid arthritis (Kjeldsen-Kragh et al., 1991; Sködstam et al., 1979), asthma (Johnson et al., 2007) and psoriasis (Jensen et al., 2016), and have been shown to prolong lifespan (Fontana et al., 2010; Picca et al., 2017). However, the molecular



mechanisms by which reduced calorie intake or fasting modulate systemic inflammation remain poorly understood.

Clinical studies performed in overweight or obese individuals undergoing caloric restriction showed a reduction of pro-inflammatory cytokines in the blood (Ho et al., 2015; Imayama et al., 2012; Loria-Kohen et al., 2013; Oh et al., 2013; Ott et al., 2017; Ramel et al., 2010; Tajik et al., 2013), and diet-induced weight loss has a superior benefit on patient systemic inflammation compared to interventional weight loss due to gastric bypass surgery (Lips et al., 2016). Although little data is available on the effect of caloric restriction on inflammation in normal-weight individuals, prior studies have shown that individuals undergoing intermittent or religious fasting have reduced basal levels of circulating pro-inflammatory cytokines including TNF α , IL-6 and IL-1 β (Aksungar et al., 2007; Faris et al., 2012; Moro et al., 2016).

Prompted by these prior results, we sought to investigate the impact of fasting on immune cell homeostasis. We first used mass cytometry to profile blood circulating cells of healthy, normal-weight humans prior to and during fasting. Strikingly, we discovered that fasting significantly reduced the number of circulating monocytes and similar results were obtained in mice. Here we describe how dietary energy intake controls the quality and quantity of blood and tissue monocytes emphasizing the link between high calorie dietary patterns and inflammatory disease outcome in patients.

RESULTS

Fasting Reduces the Pool of Circulating Monocytes in Healthy Humans and in Mice

To explore whether fasting was associated with changes in peripheral blood leukocyte populations, we profiled the composition of blood circulating immune cells of 12 healthy normal weight volunteers (mean age = 30 \pm 5 years, BMI = 22 \pm 2 kg/m²) 3 h after food intake (fed state) and after 19 h of fasting (fasting state) using cytometry by time-of-flight spectrometry (CyTOF) (Figures 1A and 1B). To control for circadian variations, all blood samples were drawn at the same time of the day (3 pm). Strikingly, we found that fasting led to significant reduction of

circulating monocytes including both CD14+ and CD16+ monocyte subsets (Figures 1C and 1D and S1A). Interestingly, in individuals with low baseline monocyte numbers, fasting did not decrease monocyte numbers below the physiologic range (Figure 1D). In addition to monocytes, a small subset of circulating dendritic cells, called CD141+ DC, was also reduced, whereas neutrophils were not significantly affected during short term fasting (Figure 1E).

We then asked whether similar changes in blood monocyte numbers also occurred in fasting mice. We chose a 4 h short-term fasting protocol during the light period (Zeitgeber [ZT]2-6) which is comparable to overnight fasting for humans and is the least stressful fasting strategy in animals (Figure S1B) (Jensen et al., 2013). Within 4 h, mice eat up to 0.5g of chow (0.2g on average) representing \sim 7% of their total 24 h food intake (Figure 1F). Intriguingly, while the frequencies of most immune cell clusters were unaffected by short-term fasting, Ly-6C^{high} pro-inflammatory monocytes were strongly reduced (Figures 1G and 1H). Ly-6C^{low} patrolling monocytes were proportionally reduced at 4 h and reduction in absolute numbers reached significance after 20 h of fasting. Prolonged fasting periods (20 h [ZT10-6], 48 h [ZT6-6]) reduced additional peripheral leukocyte populations including eosinophils, NK cells and T cells (Figures S1C and S1D). Importantly, fasting also led to significant reduction of pro-inflammatory Ly-6C^{high} monocytes in peripheral tissues including the peritoneal cavity, lung, liver, spleen and adipose tissues (Figures 1J, S1E and S1F).

Decreased numbers of circulating monocytes in fasting mice could be due to increased monocyte cell death, reduced bone marrow (BM) myelopoiesis, or reduced BM egress to the periphery. We did not detect an increased number of activated caspase-positive monocytes suggesting that the reduction of peripheral monocytes in fasting mice may not be due to increased cell death (Figure 1K). We also failed to detect decreased numbers of BM CXCR4+ monocyte precursors (Chong et al., 2016) (Figure 1L). Instead, Ly-6C^{high} monocytes accumulated in the BM of fasting mice (Figure 1M) suggesting that fasting-induced reduction of blood monocytes is due to reduced monocyte egress from the BM to the blood circulation. An important mechanism controlling BM cell egress is neuronal

Figure 1. Fasting Reduces the Number of Circulating Pro-inflammatory Monocytes in Healthy Humans and in Mice

(A) Schematic representation of the fasting experimental design.

(B to E) Blood was drawn from healthy individuals in the fed and in the fasting state and analyzed by CyTOF. (B) Multidimensional CyTOF data were clustered using viSNE. (C) Heatmap shows mean markers expression on cell clusters significantly reduced during fasting. (D and E) Paired analysis of (D) total monocytes, CD14+CD16- monocytes, and CD14-CD16+ monocytes, and (E) neutrophils in human blood during the fed and the fasted state. Dotted lines indicate physiologic range.

(F) Food intake of individual mice during 4 h between ZT2 and ZT6, and percentage of food intake between ZT2 and ZT6 with regard to 24 h food intake.

(G) CyTOF analysis of blood cells from mice that were fed or fasted for 4 h. Heatmap shows mean marker expression of clusters significantly reduced by short-term fasting.

(H) Absolute numbers of Ly-6C^{high} and Ly-6C^{low} monocytes in the blood of mice that were fed or fasted for the indicated time.

(I) Absolute numbers of neutrophils in the blood of mice that were fed or fasted for 20 h.

(J) Absolute numbers of Ly-6C^{high} monocytes in the peritoneal cavity (PC), lung, spleen, liver and adipose tissue (AT) of mice that were fed or fasted for 20 h.

(K) Percentage of caspase-3/7+ cells among Ly-6C^{high} monocytes in the blood and bone marrow (BM) of mice that were fed or fasted for 4 h.

(L) Numbers of bone marrow CXCR4+ pre-monocytes in mice that were fed or fasted for 20 h.

(M) Absolute numbers of bone marrow Ly-6C^{high} monocytes in mice that were fed or fasted for the indicated time.

(F, H to M) Every dot represents one individual animal. Horizontal bar = mean. Vertical bar = SD. Student's t test (D, E, I to L) or one-way analysis of variance (ANOVA) with Dunnett's multiple comparison test (H, M) were performed. Statistical significance is indicated by *p < 0.05, **p < 0.01, ***p < 0.001, ****p < 0.0001. ns = not significant.

See also Figure S1.

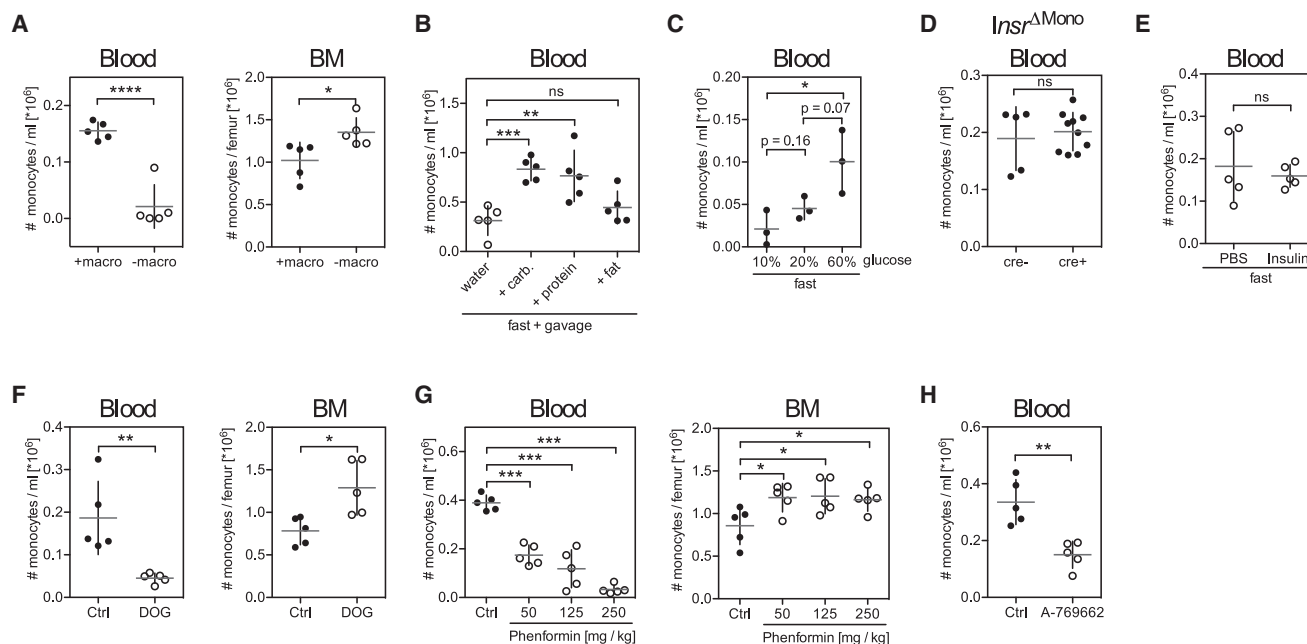


Figure 2. The Energy-sensor AMP-activated Protein Kinase (AMPK) Controls Blood Monocyte Homeostasis

(A to H) Absolute numbers of Ly-6C^{high} monocytes (A) in the blood and bone marrow (BM) of mice fed with a diet with (+macro) or without (-macro) macronutrients, (B) in the blood of fasting mice gavaged with water, isocaloric amounts of carbohydrates, protein or fat for 4 h, (C) in the blood of mice fasted for 16 h and gavaged with glucose solutions at the indicated concentrations, (D) in the blood of fed mice in which the insulin receptor has been deleted from monocytes (*Insr*^{ΔMono}), (E) in the blood of mice that were fasted for 4 h and injected with insulin 30 min prior to analysis, (F) in the blood and bone marrow of mice that were gavaged with water (Ctrl) or 2-deoxyglucose (DOG) once every hour for 4 h, (G) in the blood and bone marrow of mice that received water (Ctrl) or a single dose of phenformin 4 h before assessment, (H) in blood of mice that were gavaged with AMPK activator A-769662 4 h before analysis. (A to H) Every dot represents one individual animal. Horizontal bar = mean. Vertical bar = SD. One-way analysis of variance (ANOVA) with Tukey's multiple comparison test (C, G), or Student's t test (A, D to F, H) were performed. Statistical significance is indicated by *p < 0.05, **p < 0.01, ***p < 0.001, ****p < 0.0001. ns = not significant. See also Figure S2.

stimulation of β_3 adrenergic receptors (β_3 -AR) on BM stromal cells, which leads to reduced BM CXCL12 production and release of hematopoietic cells into the blood circulation (Méndez-Ferrer et al., 2008). Injection of the β_3 -AR agonist CL 316,243 into fasting mice partially rescued monocyte egress, but never to the same extent as in fed mice, indicating the existence of additional mechanisms suppressing egress during fasting (Figure S1G). CXCL12 BM levels were not affected by fasting suggesting that CXCL12 does not mediate fasting-induced monocyte accumulation in the BM (Figure S1H). In addition, circadian fluctuations in monocyte release or forced shifts in circadian rhythm (jetlag) did not affect fasting ability to modulate BM monocyte egress (Figures S1I, S1J, and S1K). Re-feeding mice for 4 h after an overnight fast restored monocyte numbers in the periphery (Figure S1L), showing that fasting-induced inhibition of BM egress is revoked upon food intake.

AMPK-Mediated Sensing of Dietary Energy Levels Controls the Size of the Peripheral Monocyte Pool

Fasting withdraws both dietary macronutrients (digestible carbohydrates, protein, fat) as well as essential micronutrients (vitamins, minerals, non-digestible fiber). Removal of macronutrients from the diet was sufficient to reduce the pool of circulating monocytes (Figure 2A). Conversely, oral gavage of fasting mice with isocaloric amounts of carbohydrates and proteins, but not

fat, rescued circulating monocyte numbers in the blood (Figure 2B). Importantly, the size of the monocyte pool in the blood circulation depended on the amount of carbohydrate ingested (Figure 2C).

Carbohydrate and protein intake stimulate insulin secretion, prompting us to examine the contribution of insulin in the regulation of BM monocyte egress. Genetic deletion of the insulin receptor gene in monocytes (Figure 2D) or exogenous insulin administration in fasting mice (Figure 2E) did not affect peripheral blood monocyte numbers suggesting that insulin was not responsible for BM monocyte egress. We thus hypothesized that carbohydrates and proteins might modulate peripheral monocyte numbers by altering cellular energy levels. To address this hypothesis, we used two different inhibitors of hexokinase, 2-deoxyglucose, and D-mannoheptulose, in order to block the first step in glycolysis, i.e., cellular energy production (Figures 2F and S2). Interestingly, blocking glycolysis reduced monocyte numbers to levels similar to those observed during fasting, suggesting that cellular energy levels controlled the blood circulating monocyte pool.

Mammalian 5'-AMP-activated protein kinase (AMPK) is a key cellular energy sensor triggered by an increase in the cellular AMP/ATP ratio that reflects low energy levels. Phenformin is known to elevate the cellular AMP/ATP ratio which results in AMPK activation. Strikingly, we found that phenformin

administration significantly reduced monocyte egress in a dose-dependent manner (Figure 2G). To further examine the contribution of AMPK to the regulation of blood monocyte levels we gavaged mice with a small molecule activator of AMPK (A-769662) (Figure 2H). Consistent with the data obtained with phenformin administration, we found that oral gavage with A-769662 significantly reduced the pool of blood peripheral monocytes in fed mice. Altogether these results suggest that activation of the low-energy sensor AMPK is sufficient to inhibit BM monocyte egress to the blood circulation.

Hepatic PPAR α Controls Peripheral Blood Monocyte Numbers

Peroxisome proliferator-activated receptor α (PPAR α) is a target of several nutrient-sensing pathways including AMPK and is a master transcriptional regulator in the adaptive response to fasting. PPAR α has been implicated in the anti-inflammatory effects of fasting (Wang et al., 2016; Youm et al., 2015). Strikingly, we found that fasting-induced reduction of circulating monocytes was less efficient in *Ppara*^{-/-} mice compared to wild-type mice suggesting that activation of PPAR α contributed to the regulation of monocyte homeostasis during fasting (Figure 3A). Phenformin treatment had a much more pronounced effect in *Ppara*^{+/+} mice compared to *Ppara*^{-/-} mice, indicating that AMPK-mediated reduction in peripheral monocyte numbers in fasting mice was in part mediated through PPAR α (Figure 3B).

To determine whether PPAR α mediated its effect on immune cell homeostasis by acting directly in monocytes, we generated bone marrow chimeric animals in which wild-type or *Ppara*^{-/-} bone marrow cells were injected into lethally irradiated hosts (Figure 3C). Interestingly, whereas monocyte egress was reduced in fasting wild-type mice reconstituted with *Ppara*^{-/-} BM, we failed to observe a significant reduction of blood monocytes in fasting *Ppara*^{-/-} mice reconstituted with wild-type BM, thus establishing that the control of BM monocyte egress required PPAR α expression in non-hematopoietic cells and not in monocytes.

PPAR α is expressed at higher levels in the liver (Figure S3A) and acts mainly in hepatocytes (Brocker et al., 2017), prompting us to probe the role of hepatic PPAR α in the control of peripheral monocyte numbers. Strikingly, we found that mice in which PPAR α was deleted uniquely in hepatocytes were impaired in their ability to modulate BM monocyte egress upon fasting (Figures 3D and S3B). Since modulation of BM monocyte egress upon fasting required hepatic PPAR α , we tested whether AMPK sensing of low-energy levels also occurred in hepatocytes. Importantly, we found that deletion of AMPK specifically in hepatocytes abrogated the reduction of circulating monocyte numbers upon gavage with an AMPK activator (Figure 3E). Altogether, these data establish that energy-sensing by the liver AMPK-PPAR α pathway controls the blood monocyte pool in response to caloric intake. Consistent with this idea, transcriptional analysis of hepatocytes isolated after 4 h and 12 h of fasting revealed that most differentially expressed genes were involved in metabolic processes (Figures 3F and 3G) with the top transcriptional regulator at both time-points being PPAR α (p value 3.09×10^{-25} and 1.16×10^{-46} at 4 h and 12 h, respectively). Genes involved in lipid metabolism were strongly

modulated upon short-term fasting (p value range from 4×10^{-6} - 1.27×10^{-25}) (Figures 3H and 3I) prompting us to examine whether metabolic adaptation to the fasting state played a role in the suppression of monocyte egress. However, we found that global triglyceride and ketone body levels as well as levels of most individual metabolites tested were unaffected by short-term fasting (Figures 3J, 3K, S3C and S3D). In addition, a ketogenic diet driving lipid metabolism failed to affect peripheral monocyte numbers (Figure 3L). We also interfered with fasting-induced lipid mobilization from fat depots by deleting FGF21 expression in liver, but could not detect any changes in monocyte numbers in fasting *Fgf21*^{-/-} mice compared to littermate controls (Figure 3M). In summary, these data suggest that lipid metabolites do not play a major role in the regulation of BM monocyte egress.

PPAR α Controls Steady-State CCL2 Levels

Transition from the fed to the fasting state involves changes in the plasma levels of numerous metabolic hormones. Short-term fasting induced remarkably similar changes in the plasma hormonal profile of humans and mice with increased levels of ghrelin and decreased levels of insulin, c-peptide, amylin, GIP, leptin, PP, and PYY (Figures 4A and S4A). Most interestingly, CCL2 (also known as MCP-1) plasma level was reduced in 8 out of 12 fasting human subjects. CCL2 binds to CCR2, a chemotactic receptor highly expressed on monocytes and shown to mediate monocyte BM egress (Serbina and Pamer, 2006). We also found a strong reduction of systemic CCL2 in fasting mice (Figures 4A and 4B) as well as upon administration of AMPK-activator phenformin (Figure 4C). Importantly, restoring plasma CCL2 levels through administration of recombinant protein rescued monocyte numbers in fasting mice (Figure 4D), further indicating CCL2 critical role in monocyte homeostasis during fasting. Providing glucose in fasting *Ccr2*^{-/-} mice failed to elevate blood monocyte numbers and thus did not bypass *Ccr2*-deficiency (Figure S4B).

CCL2 is produced in many tissues, but short-term fasting reduced CCL2 levels mainly in the liver, spleen, and BM among the tissues tested (Figures 4E, S4C and S4D). Strikingly, we found that fasting-induced CCL2 reduction in blood and tissues was lost in *Ppara*^{-/-} mice (Figures 4A and 4B and 4F), and phenformin treatment failed to reduce systemic CCL2 levels in PPAR α -deficient animals (Figure 4C).

Hepatocyte-specific deletion of CCL2 neither affected blood CCL2 levels nor the number of blood monocytes (Figure S4E), as was previously shown (Shi et al., 2011). Similarly, splenectomy did not significantly reduce serum CCL2 levels and did not decrease blood monocyte numbers (Figure S4F), suggesting that hepatocytes and splenocytes were not major CCL2 producers for BM monocyte egress.

Previous published data suggested that CCL2 production by BM stromal cells controlled steady-state monocyte egress (Shi et al., 2011). Accordingly, we found that BM CCL2 production correlated with peripheral monocyte numbers (Figure 4G). Immunofluorescence staining of BM tissue sections revealed that CCL2 was produced by cells in close proximity to BM sinusoids (Figure S4G) as was previously suggested (Shi et al., 2011), and BM CCL2 production correlated with CCL2 levels found in

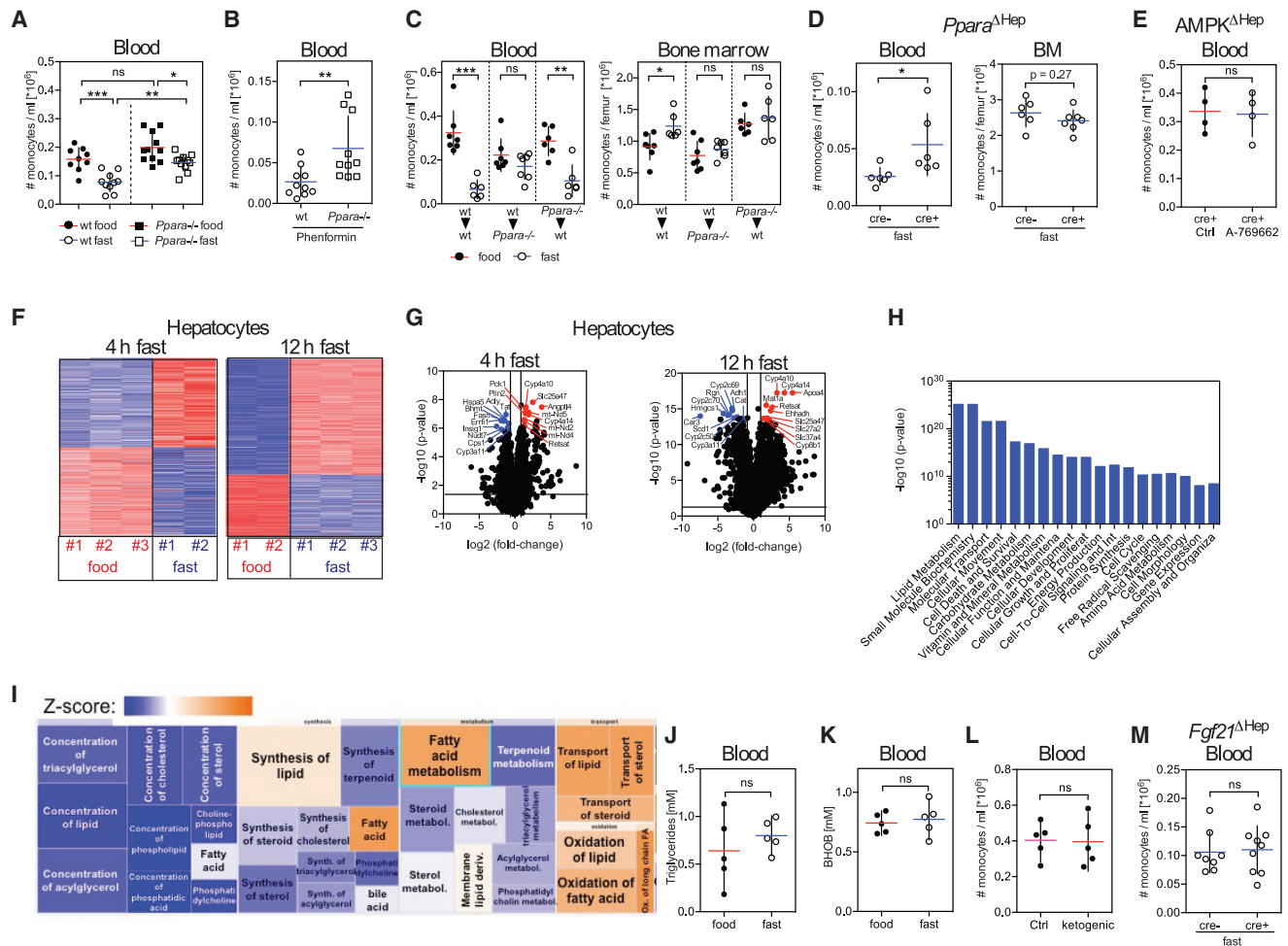


Figure 3. Liver Fasting Metabolism Regulator PPAR α Controls Peripheral Monocyte Numbers in the Steady State

(A and B) Absolute numbers of Ly-6C^{high} monocytes were measured (A) in the blood of wild-type and *Ppara*^{-/-} mice that were fed or fasted for 4 h, and (B) in the blood of wild-type and *Ppara*^{-/-} mice gavaged with phenformin 4 h prior to analysis.

(C) Bone marrow chimeric mice were generated so that wild-type mice (wt) were reconstituted with wt or *Ppara*^{-/-} bone marrow cells, and *Ppara*^{-/-} mice were reconstituted with wt bone marrow cells. Seven weeks after reconstitution half of the mice from each group were fasted for 20 h and the absolute numbers of Ly-6C^{high} monocytes in the blood and bone marrow of each bone marrow chimeric group were measured.

(D) *Alb*^{cre/cre} mice were crossed to *Ppara*^{fl/fl} mice to delete PPAR α from hepatocytes (*Ppara*^{ΔHep}) in cre⁺ mice. Graph shows absolute numbers of Ly-6C^{high} monocytes in the blood circulation and bone marrow of cre⁻ and cre⁺ mice after 20 h of fasting.

(E) *Alb*^{cre/cre} mice were crossed to *Prkaa1*^{fl/fl} mice to delete AMPK from hepatocytes (*AMPK*^{ΔHep}). Numbers of Ly-6C^{high} monocytes in blood of cre⁺ mice that were gavaged with control solvent or A-769662 4 h before analysis are shown.

(F) Heatmap shows z-scores of differentially expressed genes in hepatocytes after 4 h and 12 h of fasting.

(G) Volcano plot identifies 10 most up- and downregulated transcripts in hepatocytes after 4 h and 12 h of fasting.

(H and I) Ingenuity Pathway Analysis (IPA) of differentially expressed genes in hepatocytes after 4 h of fasting. (H) Bar chart shows most significantly altered cellular functions. (I) Detailed view of molecular functions within lipid metabolism that are affected during fasting.

(J and K) Levels of (J) triglycerides and (K) β -hydroxybutyrate (BHO) in the blood of mice that were fed or fasted for 4 h.

(L) Ly-6C^{high} monocytes in blood of mice that were fed with ketogenic or control diet for 3 weeks.

(M) *Alb*^{cre/cre} mice were crossed to *Fgf21*^{fl/fl} mice to delete *Fgf21* from hepatocytes (*Fgf21*^{ΔHep}) and cre⁻ or cre⁺ mice were fasted for 4 h. Graph shows absolute numbers of Ly-6C^{high} monocytes in the blood.

(A) Data were pooled from two experiments. (A to E, J to M) Every dot represents one individual animal. Horizontal bar = mean. Vertical bar = SD. One-way analysis of variance (ANOVA) with Bonferroni's test (A), or Student's t test (B to E, J to M) were performed. Statistical significance is indicated by * $p < 0.05$, ** $p < 0.01$, *** $p < 0.001$. ns = not significant. See also Figure S3.

blood (Figure S4H), suggesting that systemic CCL2 levels might depend on BM CCL2 production. In summary, these data indicated that fasting-induced reduction of BM CCL2 production inhibited monocyte egress to the periphery.

We next examined how fasting-driven hepatic PPAR α activation could regulate CCL2 production at distant sites. To this aim, we used mass spectrometry to measure the serum proteome during the fed and the fasting state. We found that fasting led

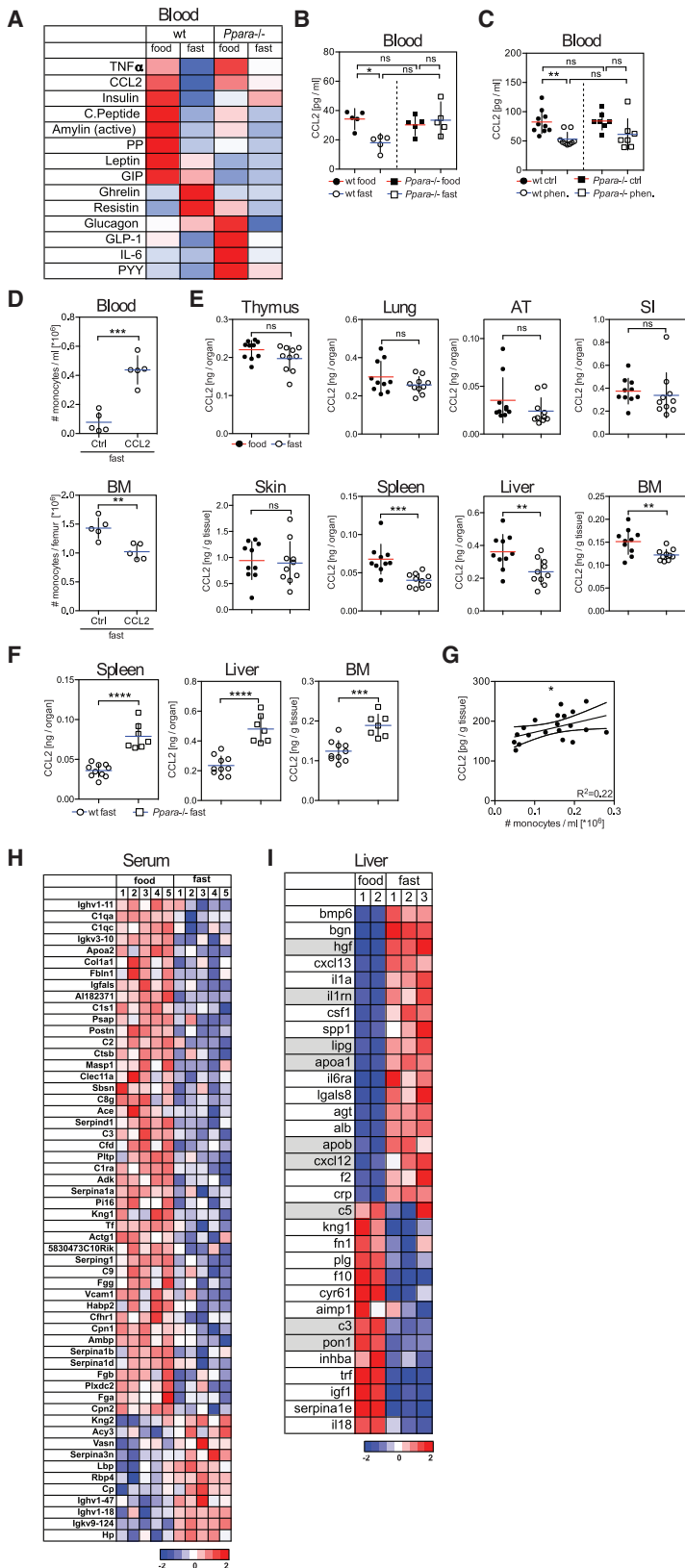


Figure 4. PPAR α Controls Tissue CCL2 Levels in the Steady-State

(A) Multiplex analysis for metabolic hormones in the blood of mice that were fed or fasted for 4 h. (B) CCL2 levels in blood of wild-type (wt) and *Ppara*^{-/-} mice that were fed or fasted for 4 h. (C) CCL2 levels in blood of wild-type (wt) and *Ppara*^{-/-} mice that were gavaged with water (Ctrl) or with a single dose of phenformin 4 h before analysis. Data were pooled from two experiments. (D) Mice were fasted for 20 h before injection of PBS or recombinant CCL2 and were analyzed 3 h after injection. Graphs show the absolute numbers of Ly-6C^{high} monocytes in the blood and bone marrow. (E) CCL2 protein in indicated tissues from wt mice that were fed or fasted for 4 h. AT = adipose tissue, SI = small intestine. (F) CCL2 protein in the indicated tissues in wt and *Ppara*^{-/-} mice that were fasted for 4 h. (G) Plot shows CCL2 production in BM versus monocyte numbers in blood. (H) Heatmap shows z-scores of significantly changing serum protein levels in mice that were fed or fasted for 20 h. (I) Differentially expressed genes in liver after 20 h of fasting were filtered using the IPA database. Heatmap shows z-scores of genes coding proteins that are annotated to be secreted to the extracellular space and to regulate CCL2. Genes annotated to be regulated by PPAR α are shaded. (B to G) Every dot represents one individual animal. Horizontal bar = mean. Vertical bar = SD. One-way analysis of variance (ANOVA) with Tukey's post test (B) or Bonferroni's post test (C), or Student's t test (D to F) were performed. Statistical significance is indicated by **p* < 0.05, ***p* < 0.01, ****p* < 0.001, *****p* < 0.0001. ns = not significant. See also Figure S4.

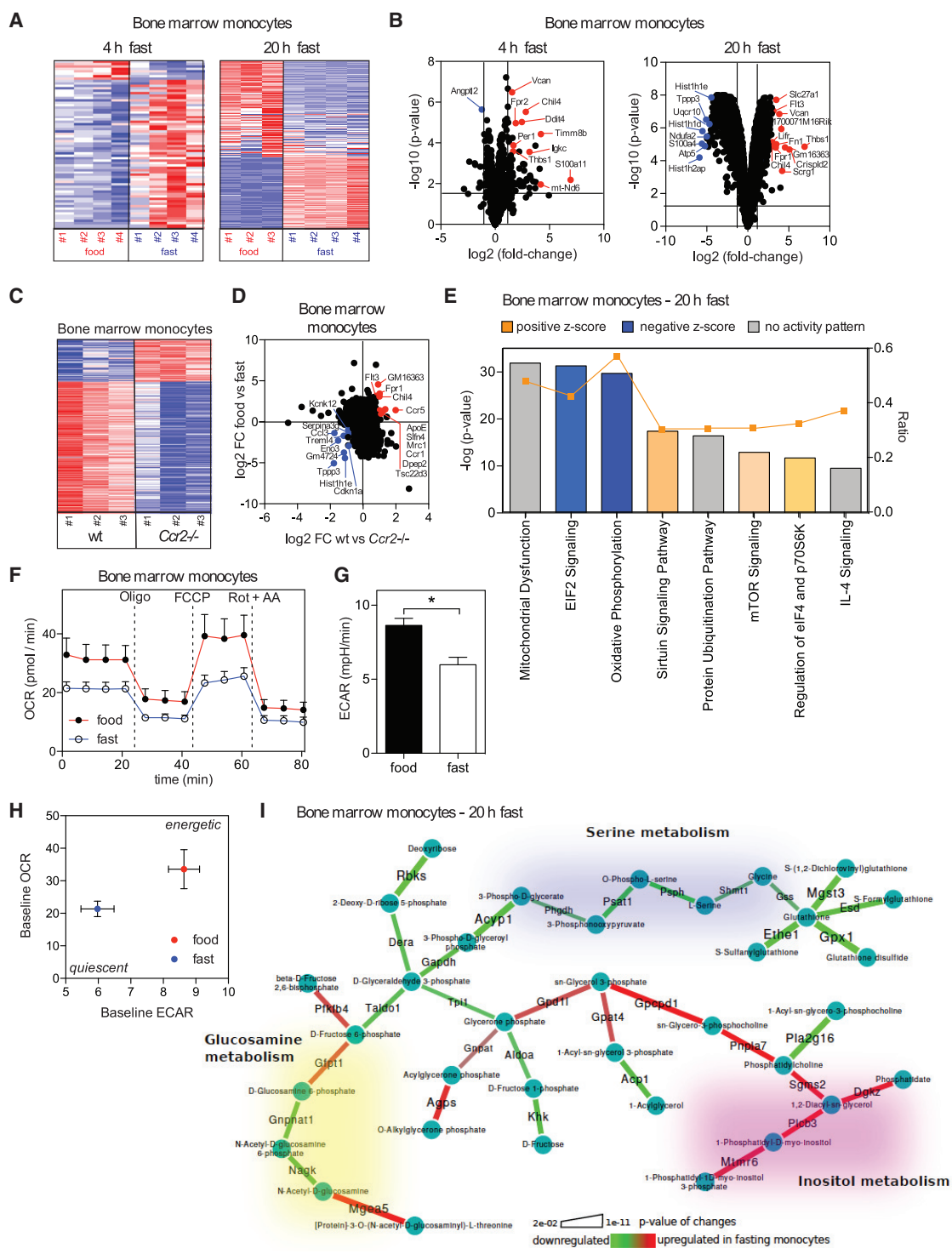


Figure 5. Fasting Modifies Monocyte Metabolic Activity

(A) Heatmaps display z-scores for differentially expressed genes in monocytes purified from the bone marrow of mice that were fed or fasted for the indicated time.
 (B) Volcano plots show top up- and downregulated transcripts in monocytes from mice that were fasted for the indicated time compared to monocytes from fed mice.
 (C) Heatmap displays z-scores for differentially expressed genes in monocytes from bone marrow of wt and *CCR2*^{-/-} mice.

(legend continued on next page)

to significant changes in serum protein levels that overlapped with differential gene expression in the fasting liver (Figures 4H and S4I), highlighting the key role of the liver in controlling the composition of the blood plasma proteome in response to dietary intake. We then mined fasting-regulated liver gene transcripts for factors that are released into the circulation and modulate CCL2 production. We found that at least 33 liver produced factors that were modulated during the fasting state were annotated to regulate CCL2 levels (Figure 4I), suggesting that the liver secretome responds to dietary intake and contains multiple circulating factors known to regulate CCL2 production.

Fasting Modifies Monocyte Metabolic Activity

In order to investigate the effect of fasting on monocyte gene expression, we profiled monocytes from the BM of fed and fasted mice (Figures 5A and 5B). Fasting had a profound effect on the monocyte gene expression profile with more than 2,700 genes being differentially expressed after 20 h of fasting. We found that the transcriptional changes in monocytes from fasting mice overlapped with those of *Ccr2*-deficient monocytes emphasizing that reduced CCL2 signaling during fasting may similarly affect the monocyte compartment (Figures 5C and 5D).

Consistent with cellular energy conservation, fasting mostly affected pathways involved in eIF2 signaling and protein ubiquitination as well as mitochondrial function and oxidative phosphorylation (Figure 5E, S5A and S5C). Accordingly, monocytes isolated from fasting mice displayed reduced basal (untreated) and maximal (FCCP-induced) oxygen consumption rates (OCR) (Figure 5F) and a reduced basal extracellular acidification (ECAR) rate (Figure 5G), resulting in a quiescent metabolic phenotype compared to monocytes from fed mice (Figure 5H). In depth metabolic network analysis revealed upregulation of inositol-triphosphate metabolism, which could be indicative of a specific signaling axis during fasting (Figures 5I, S5B and S5C). Also, we observed coordinated suppression of serine and glutathione metabolism in monocytes from fasting mice, contrary to what was described for immune cell proliferation upon activation (Ma et al., 2017). Hence, monocytes from fasting mice were reduced in their metabolic activity reflecting a quiescent functional state.

Fasting Improves Chronic Inflammatory Diseases Without Compromising Monocyte Emergency Mobilization During Acute Inflammation

Dietary interventions such as hypocaloric diets and fasting regimens improve chronic inflammatory and autoimmune disorders including multiple sclerosis and rheumatoid arthritis (Choi et al., 2017; Piccio et al., 2008). Intriguingly, gene modules associated

with “inflammation of joint” and “rheumatoid arthritis” were reduced in monocytes isolated from fasting mice (Figures S6A and S6B). Further analysis revealed strong gene regulation related to pro-inflammatory activity in monocytes upon fasting (Figure S6C). These results prompted us to examine whether fasting-induced changes in monocyte molecular program could improve chronic inflammatory disease outcome.

We focused our analysis on mice induced to develop experimental autoimmune encephalomyelitis (EAE), the main preclinical model for multiple sclerosis. EAE progression strongly depends on the recruitment of monocytes to the central nervous system (Ajami et al., 2011; King et al., 2009). *Ccr2*-deficient mice, in which monocytes are unable to exit the BM (Serbina and Pamer, 2006), were resistant to disease induction (Figure S6D), as was previously shown (Mildner et al., 2009). Similarly, mice that were subjected to intermittent fasting had reduced pro-inflammatory monocyte numbers in the blood during disease development, while neutrophil and T cell numbers were unaffected (Figures S6E, S6F and S6G). Intriguingly, we observed that intermittent fasting led to a strong reduction of monocyte accumulation in the spinal cord of mice with EAE (Figure 6A), accompanied with a significant improvement of EAE clinical course (Figure 6B), as previously shown (Cignarella et al., 2018). We also profiled infiltrating monocytes from the spinal cord of mice that were fed *ad libitum* or subjected to intermittent fasting during EAE (Figures 6C and 6D). Strikingly, purified spinal cord-infiltrating monocytes from fasted mice most significantly downregulated pro-inflammatory genes such as TNF α , IL-1 β , CXCL2 and CXCL10, and gene modules associated with monocyte pro-inflammatory activity, inflammation and inflammatory disease compared to monocytes from fed mice (Figures 6D and 6E and S6H). These data suggest that intermittent fasting leads to reduced myeloid cell accumulation in lesional sites as well as reduced monocyte inflammatory activity and is associated with improved disease outcome in EAE.

The realization that fasting reduces monocyte mobilization and monocyte functional state prompted us to ask whether fasting could also compromise acute inflammatory reactions in response to tissue injury or pathogen invasion. Both tissue restoration after injury and therapeutic immunity against *Listeria monocytogenes* critically depend on monocytes and are strongly compromised in *Ccr2*-deficient mice (Boniakowski et al., 2018; Serbina and Pamer, 2006). Strikingly, we found that short-term fasting for 20 h did not affect monocyte emergency mobilization upon *Listeria monocytogenes* infection (Figures S6I and S6J). Similar results were also obtained after long-term intermittent fasting for 6 weeks (Figures 6F and 6G and S6K). T cell numbers also remained unaltered in mice subjected to intermittent fasting

(D) Differentially expressed genes in monocytes between wt and *Ccr2*^{-/-} mice were mapped on differentially expressed genes from monocytes between mice that were fed or fasted for 20 h.

(E) Ingenuity Pathway Analysis (IPA) of differentially expressed genes in monocytes between mice that were fed and fasted for 20 h.

(F) Oxygen consumption rate (OCR) of bone marrow monocytes from mice that were fed or fasted for 20 h. Oligo = oligomycin, inhibits ATP-synthase; FCCP = carbonyl cyanide-4 (trifluoromethoxy)phenylhydrazone, mitochondrial uncoupler; Rot + AA = rotenone + antimycin A, CI and CIII inhibitors, respectively. Vertical bars = SEM.

(G) Basal extracellular acidification rate (ECAR) of bone marrow monocytes from mice that were fed or fasted for 20 h. Vertical bars = SEM.

(H) Basal OCR versus basal ECAR (mean \pm SEM for both parameters).

(I) Integrated metabolic network analysis of the transcriptional differences in monocytes between mice that were fed or fasted for 20 h. Graphical representation of the regulated metabolic subnetwork.

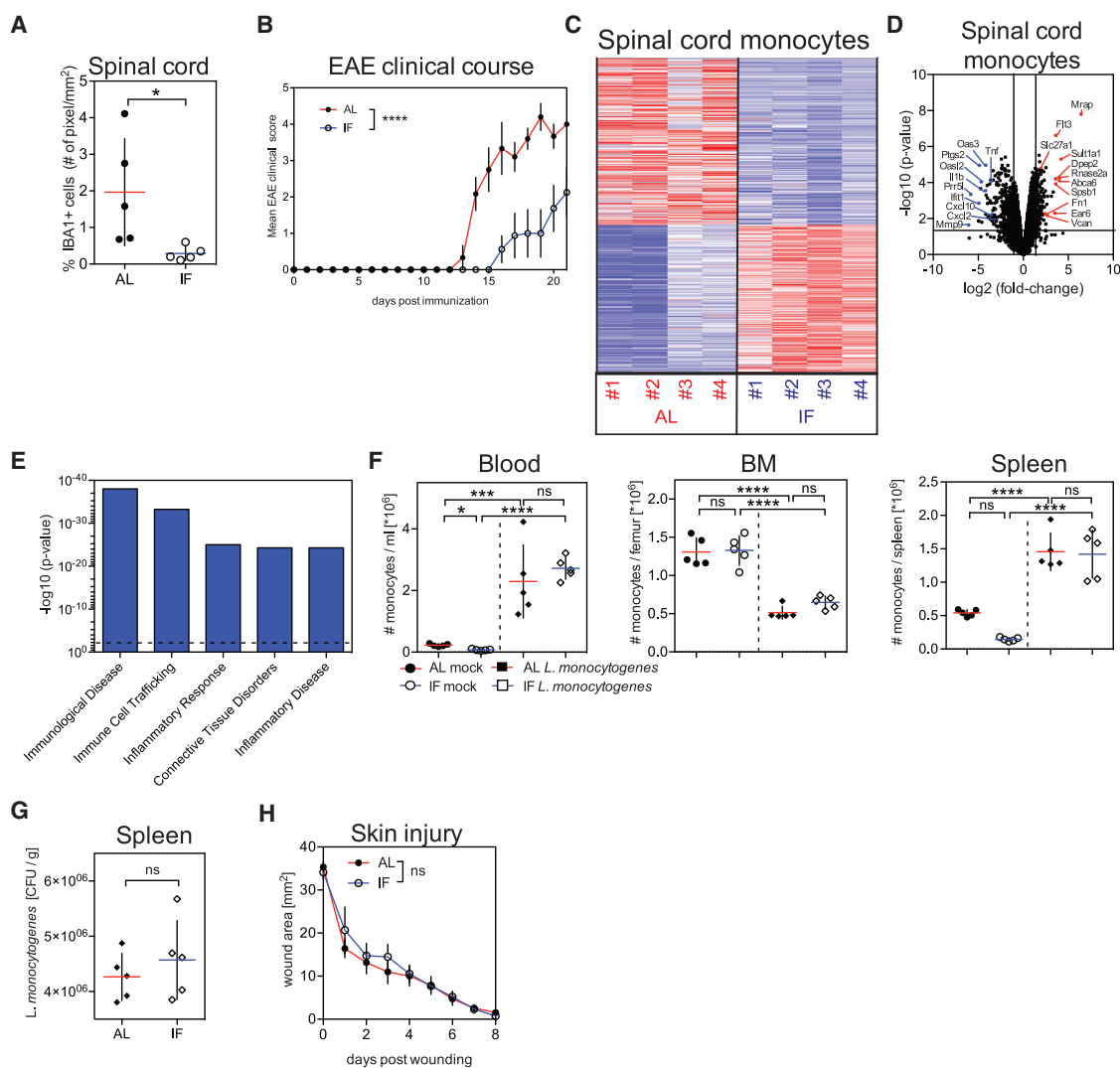


Figure 6. Fasting Improves Chronic Inflammatory Disease Outcome Without Compromising Monocyte Emergency Mobilization During Acute Inflammation

(A and B) Mice were fed *ad libitum* (AL) or subjected to intermittent fasting in 24 h cycles (IF) for 4 weeks before EAE induction and during disease development. (A) Proportion of IBA1+ myeloid cells in spinal cords and (B) and EAE clinical course.

(C, D, E) Monocytes were purified from spinal cords of mice that were induced with EAE and were fed *ad libitum* (AL) or subjected to intermittent fasting in 24 h cycles (IF) for 4 weeks before EAE induction and during disease development. (C) Heatmap displays z-scores for differentially expressed genes. (D) Volcano plots show top up- and downregulated transcripts. (E) Differentially expressed genes were analyzed using Ingenuity Pathway Analysis (IPA). Bar graph shows p values of most significantly regulated gene modules. Dotted line = threshold.

(F, G) Mice were fed *ad libitum* (AL) or subjected to intermittent fasting in 24 h cycles (IF) for 6 weeks prior to infection with *L. monocytogenes*. (F) Absolute numbers of Ly-6C^{high} monocytes in the indicated tissues. (G) *L. monocytogenes* colony-forming units (CFU) in the spleen.

(H) Wound healing kinetics in mice that were fed *ad libitum* (AL) or subjected to intermittent fasting in 24 h cycles (IF) for 4 weeks prior to wounding.

(A, F, G) Every dot represents one individual animal. Horizontal bar = mean. Vertical bar = SD. Two-way analysis of variance (ANOVA) (B, H) or One-way ANOVA with Bonferroni's post test (F) or Student's t test (A, G) were performed. Statistical significance is indicated by * $p < 0.05$, *** $p < 0.001$, **** $p < 0.0001$. ns = not significant.

See also Figure S6.

during infection (Figures S6L and S6M). Because mobilization of monocytes to the site of injury is critical for wound repair, we asked whether short-term fasting or long-term intermittent fasting could compromise wound healing. Importantly and similar to what we found in infected mice, short-term fasting or intermittent

fasting did not affect wound repair potential compared to *ad libitum* fed mice (Figures 6H and S6N). In contrast, starvation for 48 h prior to infection or skin injury compromised CCL2 expression and monocyte mobilization during *Listeria monocytogenes* infection as well as wound healing (Figures S6O, S6P, S6Q and

S6R) suggesting that starvation, in contrast to short-term or intermittent fasting could compromise antimicrobial immunity and tissue repair.

In summary, we found that intermittent fasting improved chronic inflammatory disease outcome without compromising monocyte emergency mobilization and functionality during acute inflammatory responses in response to infection or tissue injury.

DISCUSSION

Our study identified a drastic effect of short-term and intermittent fasting on the blood and tissue monocyte pool and revealed the role of dietary intake in the control of metabolic and inflammatory activity of monocytes and their egress to the blood circulation.

Egress of BM monocytes to the blood circulation is a critical step in the inflammatory cascade induced upon tissue injury (Shi and Pamer, 2011). Monocytes are important producers of pro-inflammatory cytokines and play a critical role in the induction and maintenance of inflammation. Therefore, it is conceivable that modulation of peripheral monocyte load in blood and tissues by repetitive short-term fasting or caloric restriction decreases susceptibility to pathological inflammatory disease. Indeed, circulating monocytes are increased in overweight and obese humans and caloric restriction has been shown to reduce peripheral pro-inflammatory cells leading to an overall improved inflammatory profile (Kani et al., 2017; Poitou et al., 2011). We found that fasting not only reduced the size of the circulating monocyte pool but also modified metabolic activity and gene expression patterns predicting improvement of chronic inflammatory and autoimmune disorders, such as rheumatoid arthritis and multiple sclerosis, diseases that were shown to be responsive to fasting in clinical trials (Choi et al., 2017; Darlington et al., 1986; Kjeldsen-Kragh et al., 1991; Sköldstam et al., 1979). Accordingly, caloric restriction and intermittent fasting strongly reduced the accumulation of pathogenic monocytes in the central nervous system, reduced monocyte pro-inflammatory activity, and ameliorated disease outcome in a preclinical model of multiple sclerosis (Cignarella et al., 2018; Piccio et al., 2008).

While decreased inflammatory activity is desirable in chronic autoimmune diseases, it might be devastating in response to tissue injury or pathogen invasion. Importantly, we found that short-term and intermittent fasting did not compromise tissue regeneration nor immunity against *Listeria monocytogenes*, a condition most critically dependent on monocyte emergency mobilization for the induction of therapeutic immunity. Fasting as part of physiological sickness behavior can even be beneficial in antimicrobial immunity (Wang et al., 2016). However, exaggerated fasting leading to starvation and malnutrition clearly compromises immune and tissue functions.

It has been speculated for a long time that hepatocytes might modulate monocyte BM hematopoiesis and egress (Decker et al., 2018; Serbina et al., 2012). Here we show that food energy-sensing by a liver AMPK-PPAR α pathway controls BM monocyte egress to the blood circulation. Interestingly, anti-inflammatory dietary patterns such as the Mediterranean diet are highly enriched in natural PPAR α agonists. In fact, PPAR α -dependent fasting metabolites are associated with anti-inflamma-

tory effects (Wang et al., 2016). β -Hydroxybutyrate, for example, exerts anti-inflammatory functions through binding to GPR109A or by inhibiting the NLRP3 inflammasome (Yamanashi et al., 2017; Youm et al., 2015). We have found that hepatic AMPK and PPAR α not only coordinated metabolic adaptation to fasting, but also controlled the pool of circulating inflammatory cells through the modulation of steady-state CCL2 production.

Constant or intermittent reduced calorie intake improves inflammatory and autoimmune disease outcome. Importantly, our finding that pharmacological AMPK activation regardless of caloric intake was sufficient to regulate the blood monocyte pool suggests that targeting liver energy sensors could be an innovative strategy for the prevention and treatment of chronic inflammatory and autoimmune diseases without affecting antimicrobial immunity.

Altogether, these data establish diet composition and liver energy sensors as critical regulators of the blood and tissue inflammatory tone and identify novel clinical strategies for the treatment of patients with chronic inflammatory diseases and autoimmune disorders.

STAR★METHODS

Detailed methods are provided in the online version of this paper and include the following:

- KEY RESOURCES TABLE
- LEAD CONTACT AND MATERIALS AVAILABILITY
- EXPERIMENTAL MODEL AND SUBJECT DETAILS
 - Animals
 - Human fasting trial
 - Infection with *Listeria monocytogenes*
- METHOD DETAILS
 - Diets
 - Experimental animal fasting
 - Treatments
 - Induction of experimental autoimmune encephalomyelitis (EAE)
 - Punch biopsy
 - Bone marrow chimeras
 - Flow cytometry
 - Cytometry by time-of-flight spectrometry (CyTOF)
 - Hepatocyte isolation
 - ELISA and multiplex
 - Serum metabolomics
 - qPCR
 - Metabolic measurements in monocytes
 - Transcriptome analysis
 - Serum proteomics analysis
 - Bioinformatics
- QUANTIFICATION AND STATISTICAL ANALYSIS
 - Statistics
- DATA AND SOFTWARE AVAILABILITY

ACKNOWLEDGMENTS

We thank J. Agudo, S. Offermanns, C. Buettner, S. Fried, T. E. McGraw, A. W. Ferrante and the Merad laboratory for helpful discussions. We thank J. LeBerichel for technical assistance, A. Lansky for submission of the IRB

application, the Flow Cytometry facility for technical support, the Human immune monitoring core for assistance with the multiplex assay, M. Davila for processing CyTOF data, M. Serasinghe for help with metabolic measurements in monocytes, the Stable Isotope & Metabolomics core at Albert Einstein College of Medicine for assistance with blood metabolite measurements, S. Hatem for assistance with phlebotomy and all participants of the human fasting experiment. We are grateful to Y. Belkaid for giving us the opportunity to use her laboratory at NIH and N. Bouladoux for assistance. We thank Wiegand von Hartmann GBR for designing the graphical abstract. Supported by the NIH (R01 CA154947, U24 AI118644, U19 AI128949 to M.M. and K08CA190770 to E.J.G.), The Tisch Cancer Institute (Junior Scientist Award to E.J.G.), and the German Research Council (DFG) (SFB-TRR57 P07 to M.-L.B., JO 1216/1-1 to S.J.).

AUTHOR CONTRIBUTIONS

S.J. conceived the study, designed, performed and analyzed experiments and wrote the manuscript. N.T., M.C.A., C.C., Cl.C., D.Z., T.H.W., S.N., D.H., S.H., B.B.M., A.R. and F.M. performed experiments and analyzed data. S.A.R., A.G. and M.N.A. analyzed the RNA-seq data. J.E.C., D.L. and P.S.F. provided intellectual expertise. C.N.B., P.C. and F.J.G. provided mice and intellectual expertise. L.P. and M.-L.B. designed and funded experiments. E.J.G. designed, performed, analyzed and funded experiments and wrote the manuscript. M.M. supervised and funded the study and wrote the manuscript. All authors discussed the data and edited the manuscript.

DECLARATION OF INTERESTS

The authors declare no competing interests.

Received: February 27, 2019

Revised: June 2, 2019

Accepted: July 29, 2019

Published: August 22, 2019

REFERENCES

- Ajami, B., Bennett, J.L., Krieger, C., McNagny, K.M., and Rossi, F.M. (2011). Infiltrating monocytes trigger EAE progression, but do not contribute to the resident microglia pool. *Nat. Neurosci.* *14*, 1142–1149.
- Aksungar, F.B., Topkaya, A.E., and Akyildiz, M. (2007). Interleukin-6, C-reactive protein and biochemical parameters during prolonged intermittent fasting. *Ann. Nutr. Metab.* *51*, 88–95.
- Boniakowski, A.E., Kimball, A.S., Joshi, A., Schaller, M., Davis, F.M., denDekker, A., Obi, A.T., Moore, B.B., Kunkel, S.L., and Gallagher, K.A. (2018). Murine macrophage chemokine receptor CCR2 plays a crucial role in macrophage recruitment and regulated inflammation in wound healing. *Eur. J. Immunol.* *48*, 1445–1455.
- Brandhorst, S., Wei, M., Hwang, S., Morgan, T.E., and Longo, V.D. (2013). Short-term calorie and protein restriction provide partial protection from chemotoxicity but do not delay glioma progression. *Exp. Gerontol.* *48*, 1120–1128.
- Brockner, C.N., Yue, J., Kim, D., Qu, A., Bonzo, J.A., and Gonzalez, F.J. (2017). Hepatocyte-specific PPARα expression exclusively promotes agonist-induced cell proliferation without influence from nonparenchymal cells. *Am. J. Physiol. Gastrointest. Liver Physiol.* *312*, G283–G299.
- Choi, I.Y., Piccio, L., Childress, P., Bollman, B., Ghosh, A., Brandhorst, S., Suarez, J., Michalsen, A., Cross, A.H., Morgan, T.E., et al. (2016). A Diet Mimicking Fasting Promotes Regeneration and Reduces Autoimmunity and Multiple Sclerosis Symptoms. *Cell Rep.* *15*, 2136–2146.
- Choi, I.Y., Lee, C., and Longo, V.D. (2017). Nutrition and fasting mimicking diets in the prevention and treatment of autoimmune diseases and immunosenescence. *Mol. Cell. Endocrinol.* *455*, 4–12.
- Chong, S.Z., Evrard, M., Devi, S., Chen, J., Lim, J.Y., See, P., Zhang, Y., Adraver, J.M., Lee, B., Tan, L., et al. (2016). CXCR4 identifies transitional bone marrow premonocytes that replenish the mature monocyte pool for peripheral responses. *J. Exp. Med.* *213*, 2293–2314.
- Cignarella, F., Cantoni, C., Ghezzi, L., Salter, A., Dorsett, Y., Chen, L., Phillips, D., Weinstock, G.M., Fontana, L., Cross, A.H., et al. (2018). Intermittent Fasting Confers Protection in CNS Autoimmunity by Altering the Gut Microbiota. *Cell metabolism* *27*, 1222–1235 e1226.
- Cox, J., and Mann, M. (2008). MaxQuant enables high peptide identification rates, individualized p.p.b.-range mass accuracies and proteome-wide protein quantification. *Nat. Biotechnol.* *26*, 1367–1372.
- Cox, J., Neuhauser, N., Michalski, A., Scheltema, R.A., Olsen, J.V., and Mann, M. (2011). Andromeda: a peptide search engine integrated into the MaxQuant environment. *J. Proteome Res.* *10*, 1794–1805.
- Cox, J., Hein, M.Y., Lubner, C.A., Paron, I., Nagaraj, N., and Mann, M. (2014). Accurate proteome-wide label-free quantification by delayed normalization and maximal peptide ratio extraction, termed MaxLFQ. *Mol. Cell. Proteomics* *13*, 2513–2526.
- Darlington, L.G., Ramsey, N.W., and Mansfield, J.R. (1986). Placebo-controlled, blind study of dietary manipulation therapy in rheumatoid arthritis. *Lancet* *1*, 236–238.
- Decker, M., Leslie, J., Liu, Q., and Ding, L. (2018). Hepatic thrombopoietin is required for bone marrow hematopoietic stem cell maintenance. *Science* *360*, 106–110.
- Faris, M.A., Kacimi, S., Al-Kurd, R.A., Fararjeh, M.A., Bustanji, Y.K., Mohammad, M.K., and Salem, M.L. (2012). Intermittent fasting during Ramadan attenuates proinflammatory cytokines and immune cells in healthy subjects. *Nutr. Res.* *32*, 947–955.
- Fontana, L., Partridge, L., and Longo, V.D. (2010). Extending healthy life span—from yeast to humans. *Science* *328*, 321–326.
- Haslam, D.W., and James, W.P. (2005). Obesity. *Lancet* *366*, 1197–1209.
- Ho, T.P., Zhao, X., Courville, A.B., Linderman, J.D., Smith, S., Sebring, N., Della Valle, D.M., Fitzpatrick, B., Simchowitz, L., and Celi, F.S. (2015). Effects of a 12-month moderate weight loss intervention on insulin sensitivity and inflammation status in nondiabetic overweight and obese subjects. *Horm. Metab. Res.* *47*, 289–296.
- Hughes, C.S., Foehr, S., Garfield, D.A., Furlong, E.E., Steinmetz, L.M., and Krijgsvelde, J. (2014). Ultrasensitive proteome analysis using paramagnetic bead technology. *Mol. Syst. Biol.* *10*, 757.
- Imayama, I., Ulrich, C.M., Alfano, C.M., Wang, C., Xiao, L., Wener, M.H., Campbell, K.L., Duggan, C., Foster-Schubert, K.E., Kong, A., et al. (2012). Effects of a caloric restriction weight loss diet and exercise on inflammatory biomarkers in overweight/obese postmenopausal women: a randomized controlled trial. *Cancer Res.* *72*, 2314–2326.
- Jensen, T.L., Kiersgaard, M.K., Sørensen, D.B., and Mikkelsen, L.F. (2013). Fasting of mice: a review. *Lab. Anim.* *47*, 225–240.
- Jensen, P., Christensen, R., Zachariae, C., Geiker, N.R., Schaadt, B.K., Stender, S., Hansen, P.R., Astrup, A., and Skov, L. (2016). Long-term effects of weight reduction on the severity of psoriasis in a cohort derived from a randomized trial: a prospective observational follow-up study. *Am. J. Clin. Nutr.* *104*, 259–265.
- Johnson, J.B., Summer, W., Cutler, R.G., Martin, B., Hyun, D.H., Dixit, V.D., Pearson, M., Nassar, M., Telljohann, R., Maudsley, S., et al. (2007). Alternate day calorie restriction improves clinical findings and reduces markers of oxidative stress and inflammation in overweight adults with moderate asthma. *Free Radic. Biol. Med.* *42*, 665–674.
- Kani, A.H., Alavian, S.M., Esmailzadeh, A., Adibi, P., Haghighatdoost, F., and Azadbakht, L. (2017). Effects of a Low-Calorie, Low-Carbohydrate Soy Containing Diet on Systemic Inflammation Among Patients with Nonalcoholic Fatty Liver Disease: A Parallel Randomized Clinical Trial. *Horm. Metab. Res.* *49*, 687–692.
- King, I.L., Dickendesher, T.L., and Segal, B.M. (2009). Circulating Ly-6C+ myeloid precursors migrate to the CNS and play a pathogenic role during autoimmune demyelinating disease. *Blood* *113*, 3190–3197.

- Kjeldsen-Kragh, J., Haugen, M., Borchgrevink, C.F., Laerum, E., Eek, M., Mowinkel, P., Hovi, K., and Førre, O. (1991). Controlled trial of fasting and one-year vegetarian diet in rheumatoid arthritis. *Lancet* 338, 899–902.
- Lips, M.A., van Klinken, J.B., Pijl, H., Janssen, I., Willems van Dijk, K., Koning, F., and van Harmelen, V. (2016). Weight loss induced by very low calorie diet is associated with a more beneficial systemic inflammatory profile than by Roux-en-Y gastric bypass. *Metabolism* 65, 1614–1620.
- Loria-Kohen, V., Fernández-Fernández, C., Bermejo, L.M., Morencos, E., Romero-Moraleda, B., and Gómez-Candela, C. (2013). Effect of different exercise modalities plus a hypocaloric diet on inflammation markers in overweight patients: a randomised trial. *Clin. Nutr.* 32, 511–518.
- Lumeng, C.N., and Saltiel, A.R. (2011). Inflammatory links between obesity and metabolic disease. *J. Clin. Invest.* 121, 2111–2117.
- Ma, E.H., Bantug, G., Griss, T., Condotta, S., Johnson, R.M., Samborska, B., Mainolfi, N., Suri, V., Guak, H., Balmer, M.L., et al. (2017). Serine Is an Essential Metabolite for Effector T Cell Expansion. *Cell Metab.* 25, 482.
- Manzel, A., Muller, D.N., Hafler, D.A., Erdman, S.E., Linker, R.A., and Klei-newietfeld, M. (2014). Role of “Western diet” in inflammatory autoimmune diseases. *Curr. Allergy Asthma Rep.* 14, 404.
- Méndez-Ferrer, S., Lucas, D., Battista, M., and Frenette, P.S. (2008). Haemato-poietic stem cell release is regulated by circadian oscillations. *Nature* 452, 442–447.
- Mildner, A., Mack, M., Schmidt, H., Brück, W., Djukic, M., Zabel, M.D., Hille, A., Priller, J., and Prinz, M. (2009). CCR2+Ly-6Chi monocytes are crucial for the effector phase of autoimmunity in the central nervous system. *Brain* 132, 2487–2500.
- Moro, T., Tinsley, G., Bianco, A., Marcolin, G., Pacelli, Q.F., Battaglia, G., Palma, A., Gentil, P., Neri, M., and Paoli, A. (2016). Effects of eight weeks of time-restricted feeding (16/8) on basal metabolism, maximal strength, body composition, inflammation, and cardiovascular risk factors in resistance-trained males. *J. Transl. Med.* 14, 290.
- Oh, E.G., Bang, S.Y., Kim, S.H., Hyun, S.S., Chu, S.H., Jeon, J.Y., Im, J.A., Lee, J.E., and Lee, M.K. (2013). Therapeutic lifestyle modification program reduces plasma levels of the chemokines CRP and MCP-1 in subjects with metabolic syndrome. *Biol. Res. Nurs.* 15, 48–55.
- Orr, J.S., Kennedy, A.J., and Hasty, A.H. (2013). Isolation of adipose tissue im-mune cells. *J. Vis. Exp.* 75, e50707.
- Ott, B., Skurk, T., Hastreiter, L., Lagkouvardos, I., Fischer, S., Büttner, J., Kellerer, T., Clavel, T., Rychlik, M., Haller, D., and Hauner, H. (2017). Effect of caloric restriction on gut permeability, inflammation markers, and fecal micro-biota in obese women. *Sci. Rep.* 7, 11955.
- Picca, A., Pesce, V., and Lezza, A.M.S. (2017). Does eating less make you live longer and better? An update on calorie restriction. *Clin. Interv. Aging* 12, 1887–1902.
- Piccio, L., Stark, J.L., and Cross, A.H. (2008). Chronic calorie restriction atten-uates experimental autoimmune encephalomyelitis. *J. Leukoc. Biol.* 84, 940–948.
- Poitou, C., Dalmás, E., Renovato, M., Benhamo, V., Hajduch, F., Abdennour, M., Kahn, J.F., Veyrie, N., Rizkalla, S., Fridman, W.H., et al. (2011). CD14dimCD16+ and CD14+CD16+ monocytes in obesity and during weight loss: relationships with fat mass and subclinical atherosclerosis. *Arterioscler. Thromb. Vasc. Biol.* 31, 2322–2330.
- Ramel, A., Martínez, J.A., Kiely, M., Bandarra, N.M., and Thorsdottir, I. (2010). Effects of weight loss and seafood consumption on inflammation parameters in young, overweight and obese European men and women during 8 weeks of energy restriction. *Eur. J. Clin. Nutr.* 64, 987–993.
- Serbina, N.V., and Pamer, E.G. (2006). Monocyte emigration from bone marrow during bacterial infection requires signals mediated by chemokine re-ceptor CCR2. *Nat. Immunol.* 7, 311–317.
- Serbina, N.V., Shi, C., and Pamer, E.G. (2012). Monocyte-mediated immune defense against murine *Listeria monocytogenes* infection. *Adv. Immunol.* 113, 119–134.
- Sergushichev, A.A., Loboda, A.A., Jha, A.K., Vincent, E.E., Driggers, E.M., Jones, R.G., Pearce, E.J., and Artyomov, M.N. (2016). GAM: a web-service for integrated transcriptional and metabolic network analysis. *Nucleic Acids Res.* 44 (W1), W194–W200.
- Shi, C., and Pamer, E.G. (2011). Monocyte recruitment during infection and inflammation. *Nat. Rev. Immunol.* 11, 762–774.
- Shi, C., Jia, T., Mendez-Ferrer, S., Hohl, T.M., Serbina, N.V., Lipuma, L., Leiner, I., Li, M.O., Frenette, P.S., and Pamer, E.G. (2011). Bone marrow mesen-chymal stem and progenitor cells induce monocyte emigration in response to circulating toll-like receptor ligands. *Immunity* 34, 590–601.
- Sköldstam, L., Larsson, L., and Lindström, F.D. (1979). Effect of fasting and lactovegetarian diet on rheumatoid arthritis. *Scand. J. Rheumatol.* 8, 249–255.
- Tajik, N., Keshavarz, S.A., Masoudkabar, F., Djalali, M., Sadrzadeh-Yeganeh, H.H., Eshraghian, M.R., Chamary, M., Ahmadvand, Z., Yazdani, T., and Javanbakht, M.H. (2013). Effect of diet-induced weight loss on inflammatory cyto-kines in obese women. *J. Endocrinol. Invest.* 36, 211–215.
- Ulland, T.K., Song, W.M., Huang, S.C., Ulrich, J.D., Sergushichev, A., Beatty, W.L., Loboda, A.A., Zhou, Y., Cairns, N.J., Kambal, A., et al. (2017). TREM2 Maintains Microglial Metabolic Fitness in Alzheimer’s Disease. *Cell* 170, 649–663.e13.
- Wang, A., Huen, S.C., Luan, H.H., Yu, S., Zhang, C., Gallezot, J.D., Booth, C.J., and Medzhitov, R. (2016). Opposing Effects of Fasting Metabolism on Tissue Tolerance in Bacterial and Viral Inflammation. *Cell* 166, 1512–1525.e12.
- Wei, M., Brandhorst, S., Shelehchi, M., Mirzaei, H., Cheng, C.W., Budniak, J., Groshen, S., Mack, W.J., Guen, E., Di Biase, S., et al. (2017). Fasting-mimicking diet and markers/risk factors for aging, diabetes, cancer, and car-diovascular disease. *Sci. Transl. Med.* 9, 9.
- Yamanashi, T., Iwata, M., Kamiya, N., Tsunetomi, K., Kajitani, N., Wada, N., lit-suka, T., Yamauchi, T., Miura, A., Pu, S., et al. (2017). Beta-hydroxybutyrate, an endogenous NLRP3 inflammasome inhibitor, attenuates stress-induced behavioral and inflammatory responses. *Sci. Rep.* 7, 7677.
- Youm, Y.H., Nguyen, K.Y., Grant, R.W., Goldberg, E.L., Bodogai, M., Kim, D., D’Agostino, D., Planavsky, N., Lupfer, C., Kanneganti, T.D., et al. (2015). The ketone metabolite β -hydroxybutyrate blocks NLRP3 inflammasome-mediated inflammatory disease. *Nat. Med.* 21, 263–269.
- Zubrzycki, A., Cierpka-Kmieć, K., Kmiec, Z., and Wronska, A. (2018). The role of low-calorie diets and intermittent fasting in the treatment of obesity and type-2 diabetes. *J. Physiol. Pharmacol.* 69. Published online January 21, 2019. <https://doi.org/10.26402/jpp.2018.5.02>.

STAR★METHODS

KEY RESOURCES TABLE

REAGENT or RESOURCE	SOURCE	IDENTIFIER
Antibodies		
Rat monoclonal anti-CD45 (clone 30-F11)	BioLegend	Cat#103138; RRID:AB_2563061
Rat monoclonal anti-CD45.1 (clone A20)	BioLegend	Cat#110741; RRID:AB_2563378
Rat monoclonal anti-CD11b (clone M1/70)	eBioscience	Cat#45-0112-82; RRID:AB_953560
Rat monoclonal anti-Ly-6G (clone 1A8)	BioLegend	Cat#127618; RRID:AB_1877261
Rat monoclonal anti-Ly-6C (clone AL-21)	BD Biosciences	Cat#553104; RRID:AB_394628
Rat monoclonal anti-CD115 (clone AFS98)	eBioscience	Cat#17-1152-82; RRID:AB_2314130
Rat monoclonal anti-CX3CR1 (clone SA011F11)	BioLegend	Cat#149023; RRID:AB_2565706
Rat monoclonal anti-CXCR4 (clone 2B11)	eBioscience	Cat#12-9991-82
Rat monoclonal anti-SiglecF (clone E50-2440)	BD Biosciences	Cat#552126; RRID:AB_394341
Armenian hamster anti-TCR β (clone H57-597)	eBioscience	Cat#17-5961-82; RRID:AB_469481
Rat monoclonal anti-CD4 (clone GK1.5)	eBioscience	Cat#12-0041-82; RRID:AB_465506
Rat monoclonal anti-CD8 (clone 53-6.7)	eBioscience	Cat#48-0081-82; RRID:AB_1272198
Rat monoclonal anti-CD45.2 (clone 104)	eBioscience	Cat#12-0454-82; RRID:AB_465678
Mouse monoclonal anti-human CD11c (clone Bu15)	BioLegend	Cat#337221; RRID:AB_2562834
Mouse monoclonal anti-human CD33 (clone WM53)	BioLegend	Cat#303419; RRID:AB_2562818
Mouse monoclonal anti-human CD19 (clone HIB19)	BioLegend	Cat#302247; RRID:AB_2562815
Mouse monoclonal anti-human CD45RA (clone HI100)	BioLegend	Cat#304143; RRID:AB_2562822
Mouse monoclonal anti-human CD141 (clone M80)	BioLegend	Cat#344113; RRID:AB_2562956
Mouse monoclonal anti-human CD4 (clone RPA-T4)	BioLegend	Cat#300541; RRID:AB_2562809
Mouse monoclonal anti-human CD8 (clone RPA-T8)	BioLegend	Cat#301053; RRID:AB_2562810
Mouse monoclonal anti-human CD370 (clone 8F9)	BioLegend	Cat#353802; RRID:AB_10983070
Mouse monoclonal anti-human CD16 (clone 3G8)	BioLegend	Cat#302051; RRID:AB_2562814
Mouse monoclonal anti-human CD1c (clone L161)	BioLegend	Cat#331501; RRID:AB_1088996
Mouse monoclonal anti-human CD123 (clone 6H6)	BioLegend	Cat#306027; RRID:AB_2562823
Mouse monoclonal anti-human CD66b (clone G10F5)	BioLegend	Cat#305102; RRID:AB_2661823
Anti-human CCR2 (clone K036C2)	Fluidigm	Cat#3153023B
Mouse monoclonal anti-human CD86 (clone IT2.2)	BioLegend	Cat#305435; RRID:AB_2563764
Mouse monoclonal anti-human CD27 (clone O323)	BioLegend	Cat#302839; RRID:AB_2562817
Mouse monoclonal anti-human PDL1 (clone 29E.2A3)	BioLegend	Cat#329719; RRID:AB_2565429
Mouse monoclonal anti-human CD163 (clone GHI/61)	BioLegend	Cat#333602; RRID:AB_1088991
Mouse monoclonal anti-human CD24 (clone ML5)	BioLegend	Cat#311127; RRID:AB_2563733
Mouse monoclonal anti-human CD14 (clone M5E2)	BioLegend	Cat#301843; RRID:AB_2562813
Mouse monoclonal anti-human CD56 (clone B159)	BD Biosciences	Cat#555514; RRID:AB_395904
Mouse monoclonal anti-human CD64 (clone 10.1)	BioLegend	Cat#305029; RRID:AB_2563759
Mouse monoclonal anti-human CD172a/b (clone SE5A5)	BioLegend	Cat#323801; RRID:AB_830700
Mouse monoclonal anti-human CD40 (clone 5C3)	BioLegend	Cat#334325; RRID:AB_2563750
Mouse monoclonal anti-human CCR6 (clone G034E3)	BioLegend	Cat#353427; RRID:AB_2563725
Mouse monoclonal anti-human CD25 (clone M-A251)	BioLegend	Cat#356101; RRID:AB_2561751
Mouse monoclonal anti-human CCR7 (clone G043H7)	BioLegend	Cat#353237; RRID:AB_2563726
Mouse monoclonal anti-human CD3 (clone UCHT1)	BioLegend	Cat#300443; RRID:AB_2562808
Rat monoclonal anti-human CX3CR1 (clone 2A9-1)	BioLegend	Cat#341602; RRID:AB_1595422
Mouse monoclonal anti-human CD38 (clone HB-7)	BioLegend	Cat#303535; RRID:AB_2562819
Mouse monoclonal anti-human CD16 (clone 3G8)	BioLegend	Cat#302051; RRID:AB_2562814

(Continued on next page)

Continued

REAGENT or RESOURCE	SOURCE	IDENTIFIER
Mouse monoclonal anti-human CXCR3 (clone G025H7)	BioLegend	Cat#353733; RRID:AB_2563724
Mouse monoclonal anti-human HLADR (clone L243)	BioLegend	Cat#307651; RRID:AB_2562826
Mouse monoclonal anti-human Axl (clone 108724)	R&D systems	Cat#MAB154; RRID:AB_2062558
Mouse monoclonal anti-human CCR4 (clone 205410)	R&D systems	Cat#MAB1567; RRID:AB_2074395
Rat monoclonal anti-human / anti-mouse CD11b (clone M1/70)	BioLegend	Cat#101249; RRID:AB_2562797
Rat monoclonal anti-mouse Ly-6G (clone 1A8)	BioLegend	Cat#127637; RRID:AB_2563784
Armenian hamster monoclonal anti-mouse CD11c (clone N418)	BioLegend	Cat#117341; RRID:AB_2562807
Armenian hamster monoclonal anti-mouse TCR- β (clone H57-597)	BioLegend	Cat#109235; RRID:AB_2562804
Rat monoclonal anti-mouse CD8 (clone 53-6.7)	BioLegend	Cat#100755; RRID:AB_2562796
Rat monoclonal anti-mouse CD19 (clone 6D5)	BioLegend	Cat#115547; RRID:AB_2562806
Rat monoclonal anti-mouse CD24 (clone M1/69)	BioLegend	Cat#101829; RRID:AB_2563732
Rat monoclonal anti-mouse CD25 (clone 3C7)	BioLegend	Cat#101913; RRID:AB_2562798
Rat monoclonal anti-mouse Siglec-F (clone E50-2440)	BD Bioscience	Cat#552125; RRID:AB_394340
Mouse monoclonal anti-mouse CD64 (clone X54-5/7.1)	BioLegend	Cat#139301; RRID:AB_10612757
Mouse monoclonal anti-mouse NK1.1 (clone PK136)	BioLegend	Cat#108743; RRID:AB_2562803
Rat monoclonal anti-mouse CD62L (clone MEL-14)	BioLegend	Cat#104443; RRID:AB_2562802
Rat monoclonal anti-mouse Ly-6C (clone HK1.4)	BioLegend	Cat#128039; RRID:AB_2563783
Rat monoclonal anti-mouse CD103 (clone 2E7)	BioLegend	Cat#121401; RRID:AB_535944
Rat monoclonal anti-mouse CD117 (clone 2B8)	BioLegend	Cat#105829; RRID:AB_2563710
Rat monoclonal anti-mouse / anti-human CD44 (clone IM7)	BioLegend	Cat#103051; RRID:AB_2562799
Rat monoclonal anti-mouse CD4 (clone RM4-5)	BioLegend	Cat#100561; RRID:AB_2562762
Rat monoclonal anti-mouse MHCII (clone M5/114.15.2)	BioLegend	Cat#107637; RRID:AB_2563771
Rat monoclonal anti-mouse Thy1.2 (clone 30-H12)	BioLegend	Cat#105333; RRID:AB_2563765
Rat monoclonal anti-mouse F4/80 (clone BM8)	BioLegend	Cat#123143; RRID:AB_2563767
Rat monoclonal anti-mouse IgD (clone 11-26c.2a)	BioLegend	Cat#405737; RRID:AB_2563774
Rat monoclonal anti-mouse CD169 (clone 3D6.112)	BioLegend	Cat#142401; RRID:AB_10915134
Mouse monoclonal anti-mouse CX3CR1 (clone SA011F11)	BioLegend	Cat#149002; RRID:AB_2564313
Bacterial and Virus Strains		
<i>Listeria monocytogenes</i> serovar 1/2a EGDe	Werner Goebel, Ludwig-Maximilians-University Munich	ATCC BAA-679
Chemicals, Peptides, and Recombinant Proteins		
2-deoxyglucose	Sigma-Aldrich	D6134
A-769662	Selleckchem	S2697
ACK lysis buffer	BioLegend	420301
AccuCheck Counting beads	Molecular Probes	PCB100
AIN-93G	Envigo	TD.94045
AIN-93M	Envigo	TD.94048
AIN-93G-MX	Envigo	TD.94046
AIN-93-VX	Envigo	TD.94047
BBL Brain Heart Infusion (BHI)	BD	211059
BBL Brain Heart Infusion (BHI) Agar plates	BD	255003
bovine serum albumin (BSA)	Equitech-Bio	BAH62
carboxymethylcellulose	Sigma-Aldrich	C4888
CCL2 protein	R&D systems	479-JE/CF
cellulose	Bio-Serv	#3425
CL 316,243	Sigma-Aldrich	C5976
collagenase IV	Sigma-Aldrich	C5138

(Continued on next page)

Continued

REAGENT or RESOURCE	SOURCE	IDENTIFIER
collagenase D	Roche	11088882
D-mannoheptulose	Sigma-Aldrich	97318
essential fatty acids (Udo's Oil 3*6*9)	Whole Foods	N/A
EXPRESS SYBR GreenER master mix	Invitrogen	11784200
glucose	Sigma-Aldrich	G8270
Halt Proteinase and Phosphatase inhibitor cocktail	ThermoFisher	78440
hydrogel	Clear H2O	70-01-5022
insulin (HumulinR)	Lilly	
ketogenic diet	BioServ	F3666
olive oil	Bertolli	N/A
percoll	GE Healthcare	17-0891-01
RNA to cDNA EcoDry Premix	Clontech	ST0335
phenformin HCl	Selleckchem	S2542
rodent Diet 20	PicoLab	5053
T-PER Tissue Protein Extraction Reagent	ThermoFisher	78510
Critical Commercial Assays		
AbsoluteIDQ p180 kit	Biocrates	N/A
β -hydroxybutyrate measurement kit	Cayman chemicals	700190
CCL2/JE ELISA kit	R&D systems	MJE00
Corticosterone ELISA kit	Enzo	ADI-900-097
CXCL12/SF-1 ELISA kit	R&D systems	MCX120
Hooke Kits for EAE induction in C57BL/6 mice	Hooke Laboratories	EK-2110
Human metabolic hormone multiplex kit	Millipore	HMEMAG-34K
Mouse Metabolic hormone multiplex kit	Millipore	MMHMAG-44K
Seahorse XF Cell Mito Stress Test Kit	Agilent	103015-100
Triglyceride measurement kit	Pointe Scientific	T7532
Vybrant FAM Caspase-3 and -7 assay kit	Invitrogen	V35118
Deposited Data		
RNA-seq	GEO	GSE126899
Experimental Models: Organisms/Strains		
C57BL/6	Charles River	CRL: 027
C57BL/6	The Jackson Laboratory	JAX: 000664
<i>Ppara</i> ^{-/-} mice: B6;129S4- <i>Ppara</i> ^{tm1Gonz} /J	The Jackson Laboratory	JAX: 008154
LysMcre mice: B6.129P2- <i>Lyz2</i> ^{tm1(cre)lfc} /J	The Jackson Laboratory	JAX: 004781
<i>Albcre</i> mice: B6.Cg- <i>Speer6</i> ^{-ps1Tg(Alb-cre)21Mgn} /J	The Jackson Laboratory	JAX: 003574
<i>Insr</i> ^{fl/fl} mice: B6.129S4(FVB)- <i>Insr</i> ^{tm1Khn} /J	The Jackson Laboratory	JAX: 006955
AMPK ^{fl/fl} mice: <i>Prkaa1</i> ^{tm1.1Sjm} /J	The Jackson Laboratory	JAX: 014141
<i>Fgf21</i> ^{fl/fl} mice: B6.129S6(SJL)- <i>Fgf21</i> ^{tm1.20jm} /J	The Jackson Laboratory	JAX: 022361
<i>Ccl2</i> ^{fl/fl} mice: B6.Cg- <i>Ccl2</i> ^{tm1.1Pame} /J	The Jackson Laboratory	JAX: 016849
<i>Insr</i> ^{ΔMono}	This paper	N/A
AMPK ^{ΔHep}	This paper	N/A
<i>Fgf21</i> ^{ΔHep}	This paper	N/A
<i>Ccl2</i> ^{ΔHep}	This paper	N/A
<i>Ppara</i> ^{ΔHep}	Brocker et al. 2017	N/A
Oligonucleotides		
5'- <i>Ppara</i> AGAGCCCCATCTGTCCTCTC	Sigma-Aldrich	
3'- <i>Ppara</i> ACTGGTAGTCTGCCAAACCAAA	Sigma-Aldrich	

(Continued on next page)

Continued

REAGENT or RESOURCE	SOURCE	IDENTIFIER
5'-ActB TTCCTTCTTGGGTATGGAATCCTG	Sigma-Aldrich	
3'-ActB GAGGTCTTTACGGATGTCAACG	Sigma-Aldrich	
Software and Algorithms		
Flo Jo	Tree Star Inc.	
Ingenuity pathway analysis (IPA)	QIAGEN	
Other		
Ampure XP magnetic beads	Beckman Coulter	A63880
MiniCollect tubes	Greiner	450475
Sera-Mag Speed Beads	Thermo fisher	09-981-121, 09-981-123
Z-Gel 1.1 mL serum preparation tubes	Sarstedt	41.1378.005

LEAD CONTACT AND MATERIALS AVAILABILITY

Further information and requests for resources and reagents should be directed to and will be fulfilled by the Lead Contact, Miriam Merad (Miriam.merad@mssm.edu).

EXPERIMENTAL MODEL AND SUBJECT DETAILS**Animals**

C57BL/6 were purchased from Charles River at the age of 6 weeks and housed in our facility for at least two weeks before being used in experiments. B6;129S4-*Ppara*^{tm1Gonz/J} (*Ppara*^{-/-} mice; Stock No.: 008154) were purchased from Jackson and bred in our facility. B6.129P2-*Lyz2*^{tm1(cre)lfo/J} (*LysMcre*; 004781) and B6.129S4(FVB)-*Insr*^{tm1Khn/J} (*Insr*^{fl/fl} mice; 006955) mice were crossed to delete the *Insr* gene from monocytes (*Insr*^{ΔMono} mice). B6.Cg-*Speer6*^{-ps1Tg(Alb-cre)21Mgn/J} (*Alb*^{cre/cre}; 003574) mice were crossed to *Prkaa1*^{tm1.1Sjm/J} (*AMPK*^{fl/fl}; 014141), B6.129S6(SJL)-*Fgf21*^{tm1.20jm/J} (*Fgf21*^{fl/fl}; 022361) and B6.Cg-*Ccl2*^{tm1.1Pame/J} (*Ccl2*^{fl/fl}; 016849) mice in order to generate hepatocyte-specific deletions of *AMPK*, *Fgf21* and *Ccl2* (*AMPK*^{ΔHep}, *Fgf21*^{ΔHep}, *Ccl2*^{ΔHep}). For experiments involving cre-positive conditional knockout mice, cre-negative littermates were used as controls. Mice were housed at specified pathogen free (SPF) health status in individually ventilated cages at 21–22°C and 39%–50% humidity in groups of 5 animals. Female mice at the age of 8–12 weeks were used for the experiments. Male conditional *Ppara*^{ΔHep} mice were described earlier (Brockner et al., 2017) and housed at the National Cancer Institute. Intermittent fasting experiments in mice induced with EAE were performed at Washington University in St. Louis. All animal procedures performed in this study were approved by the Institutional Animal Care and Use Committee (IACUC) of the respective institutions.

Human fasting trial

Healthy individuals (3 female and 9 male participants, mean age = 30 ± 5 years) with a BMI 18.5–25 kg/m² were admitted to the study. Leukocyte populations in human blood during the eating and the fasting state were assessed using a 2-day protocol. On the first day participants ate before 12 pm and did not consume food until after 3 pm (Figure 1A). At 3 pm blood was drawn by venipuncture (eating state) into an EDTA-coated tube. After the first blood draw participants were allowed to consume food until 8pm. Participants fasted from 8 pm until 3 pm of the following day, when the second blood sample was obtained (fasting state). Participants were allowed to drink water at all times. On both days, the total white blood count was measured using a hemocytometer (Becton Dickinson). Cells were processed for CyTOF immediately after the blood draw. The study was approved by the institutional review board and informed consent was obtained from all subjects.

Infection with *Listeria monocytogenes*

Listeria monocytogenes serovar 1/2a EGDe was a kind gift from Werner Göbel, Max von Pettenkofer-Institute, Ludwig-Maximilians-Universität München. Bacteria were grown in liquid BBL Brain Heart Infusion (BHI) medium (211059, BD) at 37°C until the culture reached OD₆₀₀ = 1. Cells were washed twice in icecold PBS, resuspended and frozen in aliquots in PBS 20% glycerol. Infectious units were determined by titration on BHI agar plates (255003, BD) Mice were infected intravenously with 3000 CFU and organs were harvested 24 hr later. Spleen homogenates were plated on BHI agar plates.

METHOD DETAILS

Diets

Mice were fed irradiated rodent Diet 20 (5053, PicoLab) *ad libitum* unless indicated otherwise and had access to reverse osmosis water from autoclaved bottles or an automatic watering system. For measurements of food intake purified diet AIN-93G (TD.94045, Envigo) was used. An AIN-93G matching fasting diet devoid of macronutrients was prepared as described before (Brandhorst et al., 2013). In brief, 0.43 mL essential fatty acids (Udo's Oil 3*6*9, Whole Foods), 10 g fiber (Cellulose #3425, Bio-Serv), 7 g AIN-93G-MX (TD.94046, Envigo), 2 g AIN-93-VX (TD.94047, Envigo) were mixed with 180.60 g hot hydrogel (70-01-5022, Clear H2O). AIN93-G intake of individual mice was measured every day for a week and the amount of fasting diet fed every 24 hr was adjusted to the previously measured 24 hr food intake. For ketogenic diet experiments ketogenic diet F3666 (BioServ) and control diet AIN-93M (TD.94048, Envigo) were used.

Experimental animal fasting

For 4 hr fasting protocols, food was removed at 9 am (ZT2), and for overnight fasting (20 hr) food was removed at 5 pm (ZT10) and the cage bedding and nesting material were changed to prevent coprophagy. For intermittent fasting, food was removed or added in 24 hr cycles between 8 and 9 am (ZT1-2). Control mice were fed *ad libitum*. Fasting and eating mice had access to water *ad libitum*.

Treatments

For β 3-AR stimulation, mice were gavaged with 1 mg/kg CL 316,243 (C5976, Sigma) dissolved in water 3 hr before analysis. For gavage of macronutrients 0.2 mL of 30% glucose (w/v) (G8270, Sigma), 30% BSA (w/v) (BAH62, Equitech-Bio) and 15% extra virgin olive oil (v/v) (Bertolli) was used as described before (Wang et al., 2016). Mice were gavaged once every hour for 4 hr. For hexokinase inhibition mice were gavaged with 750 mg/kg 2-deoxyglucose (D6134, Sigma) or 170 mg/kg D-mannoheptulose (97318, Sigma) in water once every hour for 4 hr. For pharmacological AMPK activation mice were gavaged with a single dose of 50 mg/kg phenformin HCl (S2542, Selleckchem) dissolved in water unless indicated otherwise, or 50 mg/kg A-769662 (S2697, Selleckchem) suspended in 1% carboxymethylcellulose (C4888, Sigma), and blood and bone marrow were analyzed 4 hr later. Insulin (HumulinR, Lilly) was injected intraperitoneally into mice that fasted for 3 hr at a dose of 1 unit/kg. For CCL2 reconstitution mice were fasted overnight and received 80 ug/kg CCL2 protein (479-JE/CF, R&D) in PBS intravenously 3 hr before analysis. 4 hr treatments were started at 9am (ZT2), 3 hr treatments at 10am (ZT3) in the home cage and mice were analyzed at 1pm (ZT6).

Induction of experimental autoimmune encephalomyelitis (EAE)

Mice were fasted in 24 hr cycles for 4 weeks before induction of EAE (Cignarella et al., 2018). For disease induction, a commercially available kit was used according to the manufacturer's instructions (EK-2110, Hooke Laboratories).

Punch biopsy

The dorsal skin of mice was shaved and 6 mm biopsy punches (Miltex) were used to make full-thickness wounds. Wound closure was assessed macroscopically with an engineer's caliper daily.

Bone marrow chimeras

Bone marrow chimeras were generated by transplantation of 2×10^6 bone marrow donor cells into lethally irradiated (2×6.5 Gy) recipient mice. Mice were kept on sulfamethoxazole / trimethoprim (STI Pharma) for 3 weeks and analyzed 7 weeks after the transfer.

Flow cytometry

Unless indicated otherwise organs were harvested at 1 pm (ZT6). Single cell suspensions were obtained from spleens by passing the organ through a 100 μ m cell strainer and from liver and lung after digestion with 0.5mg / ml collagenase IV (C5138, Sigma) at 37°C for 45 and 30 min, respectively. For liver tissue, nonparenchymal cells were enriched by centrifugation in 35% Percoll (17-0891-01, GE Healthcare) for 30 min at 1,300 rcf. Single cell suspension from adipose tissue was prepared as described before (Orr et al., 2013). In brief, gonadal fat pads were cut into small pieces and digested in collagenase IV 10 mM CaCl₂ at 37°C on a shaker at 100 rpm for 20 min. Digested tissue was triturated and passed through a 100 μ m filter. Liver, lung, adipose tissue, spleen and bone marrow single cell suspensions were incubated with ACK lysing buffer (420301, BioLegend) for 3 min at room temperature. Blood was drawn retro-orbitally or from liver sinus into EDTA-coated MiniCollect tubes (450475, Greiner). 50 μ l blood were transferred into 2 mL FACS buffer (PBS w/o Ca²⁺ and Mg²⁺ supplemented with 2% heat inactivated FBS and 5 mM EDTA) and treated twice with ACK lysing buffer for 5 min at room temperature. For flow cytometry, cells were stained in FACS buffer with mAbs specific to CD45 (clone 30-F11, BioLegend), CD45.1 (A20, eBioscience), CD45.2 (104, eBioscience), CD11b (M1/70, eBioscience), Ly-6G (1A8, BioLegend), Ly-6C (AL-21, BD Biosciences), CD115 (AFS98, eBioscience), CX3CR1 (SA011F11, BioLegend), CXCR4 (2B11, eBioscience), SiglecF (E50-2440, BD Biosciences), TCR β (H57-597, eBiosciences), CD4 (GK1.5, eBiosciences), CD8 (53-6.7, eBiosciences) for 20 min on ice. Proapoptotic cells were stained for Caspase-3/7 activation using the Vybrant FAM Caspase-3 and -7 assay kit (V35118, Invitrogen) following the manufacturer's instructions. Dead cells were excluded using DAPI staining (D1306, Life technologies) and AccuCheck counting beads (PCB100, Molecular Probes) were used for quantification of absolute cell numbers. Multiparameter

analysis was performed on an LSR Fortessa II (Becton Dickinson) using the FACSDiva software and data were analyzed using the Flo Jo software (Tree Star Inc.).

Cytometry by time-of-flight spectrometry (CyTOF)

All mass cytometry reagents were purchased from Fluidigm Inc. unless otherwise noted. Individual human whole blood samples were stained with a cocktail of the following metal labeled antibodies (all antibodies sourced from Biolegend and conjugated in house using Fluidigm X8 MaxPar conjugation kits unless otherwise noted):

CD11c 115 In (Bu15), CD33 141 Pr (WM53), CD19 142 Nd (HIB19), CD45RA 143 Nd (HI100), CD141 144 Nd (M80), CD4 145 Nd (RPA-T4), CD8 146 Nd (RPA-T8), CD370 147 Sm (8F9), CD16 148 Nd (3G8), CD1c 150 Nd (L161), CD123 151 Eu (6H6), CD66b 152 Sm (G10F5), CCR2 153 Eu (K036C2; Fluidigm), CD86 154 Sm (IT2.2), CD27 155 Gd (O323), PDL1 156 Gd (29E.2A3), CD163 158 Gd (GHI/61), CD24 159 Tb (ML5), CD14 160 Gd (M5E2), CD56 161 Dy (B159; BD Biosciences), CD64 162 Dy (10.1), CD172a/b 163 Dy (SE5A5), CD40 164 Dy (5C3), CCR6 165 Ho (G034E3), CD25 166 Er (M-A251), CCR7 167 Er (G043H7), CD3 168 Er (UCHT1), CX3CR1 169 Tm (2A9-1), CD38 170 Er (HB-7), CD161 171 Yb (HP-3G10), CXCR3 173 Yb (G025H7), HLADR 174 Yb (L243), Axl 175 Lu (108724; R&D), CCR4 176 Yb (205410; R&D), CD11b 209 Bi (M1/70). The titrated panel of antibodies was added directly to 400 μ l of whole blood and incubated for 20 min at RT. The blood was then fixed and lysed using BD FACS Lysing solution, and the cells were post-fixed for 30 min with freshly diluted 1.6% formaldehyde in PBS containing a 1:4000 dilution of Ir nucleic acid intercalator to label all nucleated cells. Staining cells were stored in PBS containing 0.1% BSA until immediately prior to acquisition.

Individual mouse blood samples were barcoded with anti CD45 antibodies (clone A20) and pooled for batched analysis. Samples were stained with a cocktail of the following metal-conjugated antibodies from Biolegend unless noted otherwise:

Ly-6G 141 Pr (clone 1A8), CD11c 142 Nd (N418), TCRb 143 Nd (H57-597), CD8 168 Er (53-6.7), CD11b 148 Nd (M1/70), CD19 149 Sm (6D5), CD24 144 Nd (M1/69), CD25 151 Eu (3C7), Siglec-F 152 Sm (E50-2440; BD Bioscience), CD64 156 Gd (X54-5/7.1), NK1.1 170 Er (PK136), CD62L 160 Gd (MEL-14), Ly-6C 162 Dy (HK1.4), CD103 161 Dy (2E7), CD117 166 Er (2B8), CD44 171 Yb (IM7), CD4 172 Yb (RM4-5), MHCII 174 Yb (M5/114.15.2), Thy1.2 113 In (30-H12), F4/80 146 Nd (BM8), IgD 150 Nd (11-26c.2a), CD169 154 Sm (3D6.112), CX3CR1 176 Yb (SA011F11), Cisplatin 195 Pt.

The cells were stained for 30 min on ice, and then washed. After antibody staining, the cells were incubated with cisplatin for 5 min at RT as a viability dye for dead cell exclusion. Cells were fixed in PBS containing 1.6% formaldehyde and a 1:4000 dilution of Ir nucleic acid intercalator to label all nucleated cells.

Immediately prior to acquisition, the cells were washed in PBS, then in diH₂O and resuspended in diH₂O containing a 1/10 dilution of Equation 4 Element Calibration beads. After routine instrument tuning and optimization, the samples were acquired on a CyTOF2 Mass Cytometer equipped with a Super Sampler fluidics system (Victorian Airships) at an acquisition rate of < 500 events /s. The resulting FCS files were concatenated and normalized using a bead-based normalization algorithm in the CyTOF acquisition software and uploaded to Cytobank for analysis. FCS files were manually pre-gated on Ir193 DNA⁺ CD45⁺ events, excluding dead cells, doublets and DNA-negative debris, and the gated populations were then analyzed using viSNE (Amir el et al., 2013) and Phenograph.

Hepatocyte isolation

For primary hepatocyte isolation the inferior vena cava was cannulated and livers were perfused with calcium-free salt solution containing 0.5 mM EGTA followed by perfusion with 90 mL of a 0.02% collagenase D solution (11088882, Roche) at RT. After digestion livers were gently minced on a Petri dish and passed through a 70 μ m cell strainer. Hepatocytes were washed three times in PBS and centrifuged at 50xg for 3 min. Cells were resuspended in Trizol at 200,000 cells / ml for further analysis.

ELISA and multiplex

Blood serum was isolated using Z-Gel 1.1 mL serum preparation tubes (41.1378.005, Sarstedt) according to the manufacturer's instructions. Tissue for protein measurements was snap frozen in liquid nitrogen. 50-100 mg tissue were added to 10x the weight T-PER Tissue Protein Extraction Reagent (78510, ThermoFisher) containing Halt Proteinase and Phosphatase inhibitor cocktail (78440, ThermoFisher). Tissue was homogenized using a 5 mm steel bead (QIAGEN) and a TissueLyser II (QIAGEN) at 30 hz for 2 min (spleen, liver, adipose tissue, pancreas, thymus, kidney), 5 min (muscle, heart, lung, cecum, large intestine, small intestine) or 10 min (skin, stomach). Debris was pelleted and supernatant used for assays. Bone marrow was prepared by flushing 2 femurs with 500 μ l PBS. After pelleting the cells, supernatant was used for BMEF measurements, while cells were taken up in T-PER lysis buffer, underwent one freeze-thaw cycle and debris was pelleted. For measurement of serum and tissue chemokine levels commercially available ELISA kits for CCL2/JE (MJE00, R&D) and CXCL12/SF-1 (MCX120, R&D) were used. For measurement of blood stress hormone corticosterone an ELISA kit was used (ADI-900-097, Enzo). Multiplex was performed using a kit for mouse metabolic hormones (MMHMAG-44K, Millipore) and human metabolic hormones (HMEMAG-34K, Millipore).

Serum metabolomics

Commercially available kits were used to measure total serum triglycerides (T7532, Pointe Scientific) and β -hydroxybutyrate (700190, Cayman chemicals) according to the manufacturer's instructions. Measurements for metabolites in mouse plasma were performed using the AbsoluteIDQ p180 kit (Biocrates) by the Stable Isotope & Metabolomics Core at Albert Einstein College of Medicine, New York.

qPCR

Conventional reverse transcription was performed using the RNA to cDNA EcoDry Premix (ST0335, Clontech) in accordance with the manufacturer's instructions. qPCR was performed on a CFX384 Touch Real-Time PCR detection system (Bio Rad) using EXPRESS SYBR GreenER master mix (11784200, Invitrogen) and primers for *Ppara* (5'-*Ppara* AGAGCCCCATCTGTCCTCTC, 3'-*Ppara* ACTGG TAGTCTGCAAAACCAAA) and *Actb* (5'-*Actb* TTCCTTCTTGGGTATGGAATCCTG, 3'-*Actb* GAGGTCTTTACGGATGTCAACG) as follows: one cycle at 95°C (10 min), 40 cycles of 95°C (15 s) and 58°C (1 min). Expression of *Actb* was used as a standard. The average threshold cycle number (CRtR) for each tested mRNA was used to quantify the relative expression: $2^{[Ct(Actb)-Ct(Ppara)]}$.

Metabolic measurements in monocytes

For metabolic measurements 250,000 monocytes / well were plated in a XF96 plate. We used the Seahorse XF Cell Mito Stress Test Kit (103015-100, Agilent) according to the manufacturer's instructions.

Transcriptome analysis

Transcript abundances were quantified using the Ensembl GRCm38 cDNA reference using Kallisto version 0.44.0. Transcript abundances were summarized to gene level using tximport. Expression matrices were filtered for only transcripts with greater than 5 TPM in all replicates of at least one condition. Differential expression statistics between different conditions were calculated using limma/voom method in R with TMM normalization. P values were adjusted for multiple testing by Benjamini-Hochberg correction.

Serum proteomics analysis

For serum proteomics analysis, samples were prepared following a modified (SP3) magnetic bead based strategy (Hughes et al., 2014). 150 µg serum protein were added to 100 µg magnetic beads (1:1 combination of Beckman Coulter (Ampure XP, A63880) and Thermo Fisher (Sera-Mag Speed Beads, 09-981-121, 09-981-123) in 100 µl lysis buffer (5 mM EDTA, 5 mM EGTA, 10 mM NaOH, protease inhibitor (1x complete Protease Inhibitor Cocktail-EDTA (Roche)), 10 mM DTT, 4% SDS, 10 mM HEPES at pH = 8.5) and subjected to 15 min sonication at 4°C (level 5, Bioruptor, Diagenode). After acidification with 8 µl 0.05% formic acid, samples were incubated for 5 min at 95°C and cysteine residues were alkylated by adding 11 µl 0.55 M 2-Iodoacetamide followed by 30 min incubation at 21°C in the dark. The reaction was quenched with 11 µl 0.5 M dithiothreitol and samples were further acidified with 40 µl 1% formic acid. Next, acetonitrile was added to a final concentration of 50% and samples were shaken (Thermoshaker at 500 rpm) for 10 min at 21°C to facilitate protein binding to the beads. The magnetic beads were separated from the supernatant using a magnetic rack and the supernatant was discarded. Beads/proteins were washed twice with 600 µl 70% ethanol followed by a single washing step with 500 µl 100% acetonitrile. After beads/proteins were dried for 30 s, 200 µl of digestion buffer (200 µl 4 mM HEPES pH = 8.0) was added. Samples were briefly sonicated to disperse bead pellets and LysC and Trypsin were added (3 µg each) and proteins were digested for 14 hr at 37°C (Thermoshaker at 500 rpm). The sample volume was reduced to 50 µl in a speedvac at 21°C and 1.1 mL acetonitrile was added resulting in a final concentration of at least 95%. Samples were briefly vortexed and shaken (Thermoshaker at 500 rpm) for 10 min at 21°C. Beads were washed with 180 µl 100% acetonitrile and reconstituted in 200 µl H₂O. To allow peptides to transfer to the aqueous phase, samples were agitated (Thermoshaker at 500 rpm) for 10 min at 21°C. The supernatant was transferred to a PCR tube and dried down in a speedvac at 21°C and peptides were reconstituted in 50 µl 0.1% formic acid.

For LC-MS/MS analysis, peptides were loaded onto 50-cm columns packed in-house with C18 1.9 µm ReproSil particles (Dr. Maisch GmbH), with an EASY-nLC 1000 system (Thermo Fisher Scientific) coupled to the MS (Q Exactive HF, Thermo Fisher Scientific) and the column oven (Sonation) set to 60°C. Peptides were eluted in a 95 min gradient of 5 to 30% from A (0.1% formic acid) to buffer B (60% ACN, 0.1% formic acid) at a flow rate of 300 nL/min. A data-dependent acquisition MS method was used, with MS scans (300 to 1650 m/z, R = 60,000 at 200 m/z) at a target of 3×10^6 ions was first performed, followed by 15 data-dependent MS/MS scans with higher-energy collisional dissociation [target 105 ions, max ion fill time 28 ms, isolation window 1.4 m/z, normalized collision energy 27%, R = 15,000 at 200 m/z]. Unassigned, single and more than sixfold charged ions were excluded from sequencing and the dynamic exclusion was set to 30 s.

MS/MS raw data were processed by the MaxQuant software version 1.6.2.10 (Cox and Mann, 2008) and peptide fragments were searched against the mouse Uniprot database by the Andromeda search engine (Cox et al., 2011) with cysteine carbamidomethylation as a fixed modification and N-terminal acetylation and methionine oxidations as variable modifications. Protein identification required at least one razor peptide and a minimum ratio count of 1 was required for quantification using MaxLFQ (Cox et al., 2014). Peptide identifications were matched across samples by nonlinear retention time alignment. Data were filtered for common contaminants, peptides only identified by site modification, hits to the reverse database and at least three measured values in at least one of the experimental groups. The remaining missing values were imputed and significantly up-or-downregulated proteins were determined by Student's t test.

Bioinformatics

For bioinformatical analysis of transcriptional profiling data we used the ingenuity pathway analysis portal (QIAGEN). For identification of potential metabolic modules differentially regulated in monocytes during the fed and fasting state a method called GATOM (from Genes, Metabolites and Atoms) was used (Sergushichev et al., 2016; Ulland et al., 2017). GATOM uses carbon atomtransition

graph. It is a graph where each vertex is an atom of a metabolite and an edge connects two atoms A1 and A2 of metabolites M1 and M2 if there is a reaction R with M1 and M2 on different sides of equation and atom A1 of M1 transforms to atom A2 of M2. Each element (vertex or edge) of the graph is assigned with a weight that is positive if the data support its importance or negative if not. The weight could be derived from statistical test p values, such as differential expression, carried out for transcriptional or metabolic data.

QUANTIFICATION AND STATISTICAL ANALYSIS

Statistics

Unless indicated otherwise, data are shown from one out of at least two experiments with $n > 3$ mice per group. Data are plotted for individual animals with group means (horizontal lines) and standard deviation (SD, vertical lines). Statistical analysis was performed using Prism 5 (GraphPad Software). Depending on the dataset two-tailed Student's t test or TWO- or ONE-way ANOVA with Tukey's, Dunnett's or Bonferroni's multiple comparison tests were applied to determine significance, and the test used for statistical analysis is indicated in the figure legend. Statistical significance is indicated by * $p < 0.05$, ** $p < 0.01$, *** $p < 0.001$, **** $p < 0.0001$. ns = not significant.

DATA AND SOFTWARE AVAILABILITY

RNA-seq data are available at the GEO repository under the accession number GSE126899.

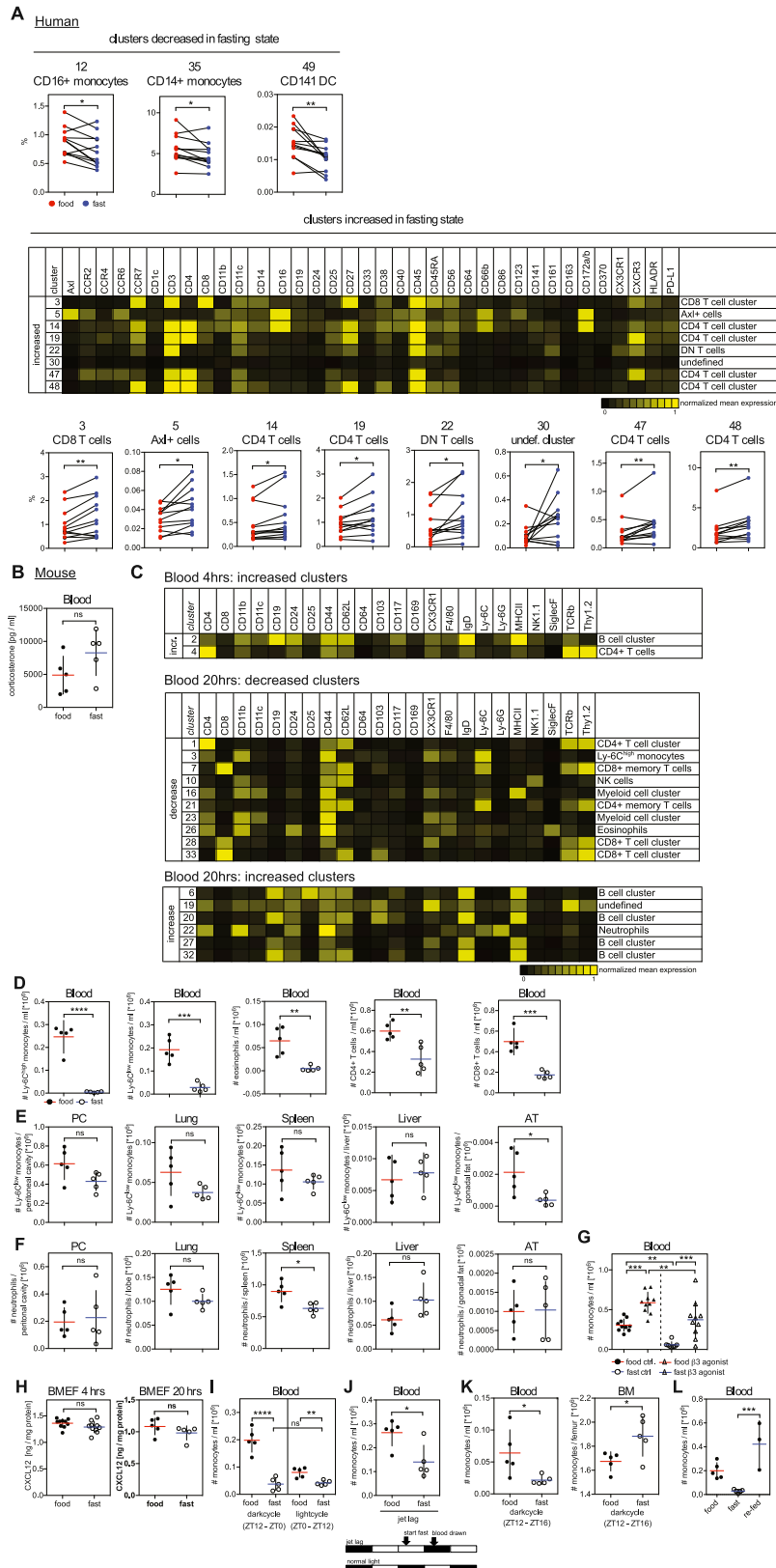


Figure S1. Profiling of Leukocyte Populations in the Fed and the Fasting State in Healthy Humans and in Mice. Related to Figure 1

(A) Blood was drawn from healthy humans in the fed and in the fasting state and analyzed by CyTOF as described in Figure 1. Multidimensional CyTOF data were clustered using tSNE. Individual representation of each significantly modulated cell cluster. Dots and lines represent paired samples from the fed and fasting state of individual participants. Heatmap shows marker expression on significantly increased clusters.

(B) Corticosterone levels in blood of mice that were fed or fasted for 4 hr.

(C) CyTOF analysis of blood from mice that were fed or fasted for 4 hr and 20 hr. Heatmaps show mean marker expression on significantly changing cell clusters during fasting.

(D) Quantification of Ly-6C^{high} and Ly-6C^{low} monocytes, eosinophils, CD4⁺ and CD8⁺ T cells in the blood of mice that were fed or fasted for 48 hr.

(E and F) Quantification of (E) Ly-6C^{low} monocyte, and (F) neutrophil numbers in peritoneal cavity (PC), lung, spleen, liver, adipose tissue (AT) of mice that were fed or fasted for 20 hr.

(G) Numbers of Ly-6C^{high} monocytes in blood from mice that were fed or fasted for 20 hr, or fed or fasted for 20 hr and gavaged with β 3 agonist CL 316,243. Data were pooled from two experiments.

(H) Level of CXCL12 in bone marrow extracellular fluid (BMEF) from mice that were fed or fasted for the indicated time.

(I) Absolute numbers of Ly-6C^{high} monocytes in the blood of mice that were fasted for 12 hr either during the light- or the darkcycle.

(J) One darkcycle was replaced by a lightcycle prior to analysis as depicted. Absolute numbers of Ly-6C^{high} monocytes in the blood are shown.

(K) Absolute numbers of Ly-6C^{high} monocytes in the blood and bone marrow of mice that were fed or fasted for 4 hr during the darkcycle.

(L) Absolute numbers of Ly-6C^{high} monocytes in the blood of mice that were fed, fasted for 20 hrs or fasted and re-fed for 4 hr.

(B, D to L) Every dot represents one individual animal. Horizontal bar = mean. Vertical bar = SD. Student's t test (A, B, D to F, H, J to L) or One-way analysis of variance (ANOVA) with Bonferroni's test (G, I) were performed. Statistical significance is indicated by *p < 0.05, **p < 0.01, ***p < 0.001, ****p < 0.0001. ns = not significant.

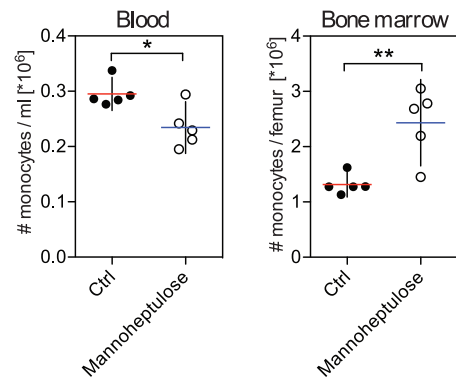


Figure S2. Inhibition of Glycolysis Reduces Circulating Monocyte Numbers. Related to Figure 2

Absolute numbers of Ly-6C^{high} monocytes in the blood and bone marrow of mice that were gavaged with water (Ctrl) or D-mannoheptulose once every hour for 4 hr. Every dot represents one individual animal. Horizontal bar = mean. Vertical bar = SD. Student's t test. Statistical significance is indicated by *p < 0.05, **p < 0.01.

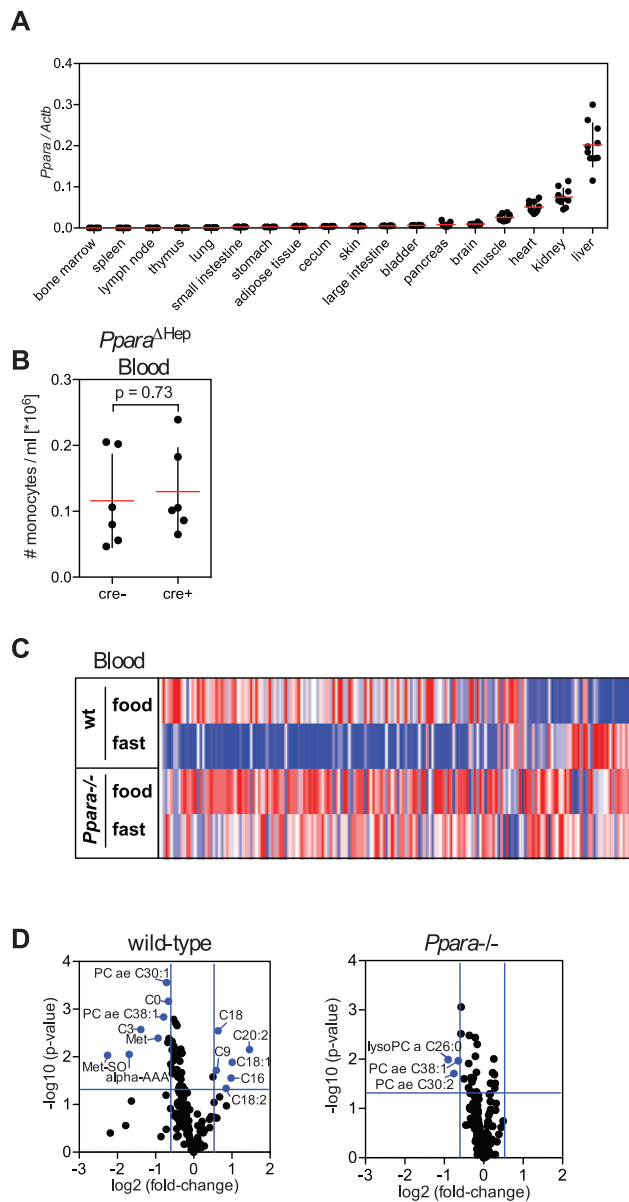


Figure S3. Profiling of Serum Metabolites in Short-term Fasted Mice. Related to Figure 3

(A) QPCR for *Ppara* mRNA on indicated tissues. Every dot represents one individual animal. (B) *Alb*^{cre/cre} mice were crossed to *Ppara*^{fl/fl} mice to delete PPAR α from hepatocytes (*Ppara*^{ΔHep}) in cre+ mice. Graph shows absolute numbers of Ly-6C^{high} monocytes in the blood circulation of cre- and cre+ mice that were fed *ad libitum*. Significance was tested using Student's t test.

(C and D) 188 metabolites were measured in blood from wt and *Ppara*^{-/-} mice that were fed or fasted for 4 hr. (C) Heatmap shows z-scores for individual metabolites. (D) Fold-changes and p values for individual metabolites between wt and *Ppara*^{-/-} mice that were fed or fasted for 4 hr are represented on a volcano plot.

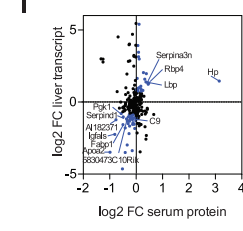
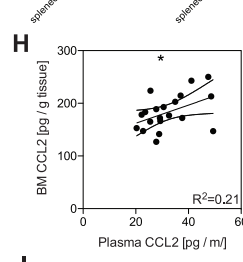
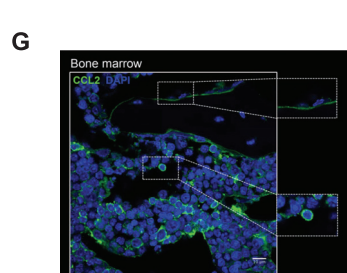
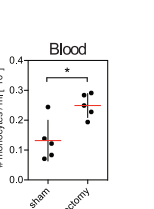
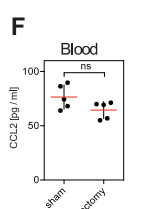
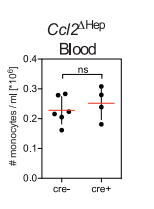
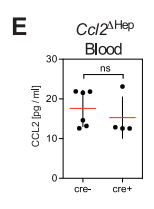
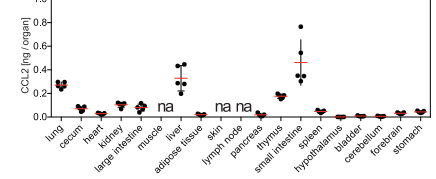
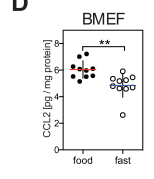
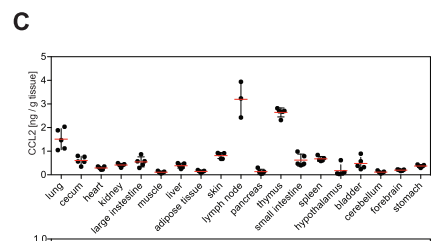
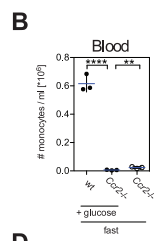
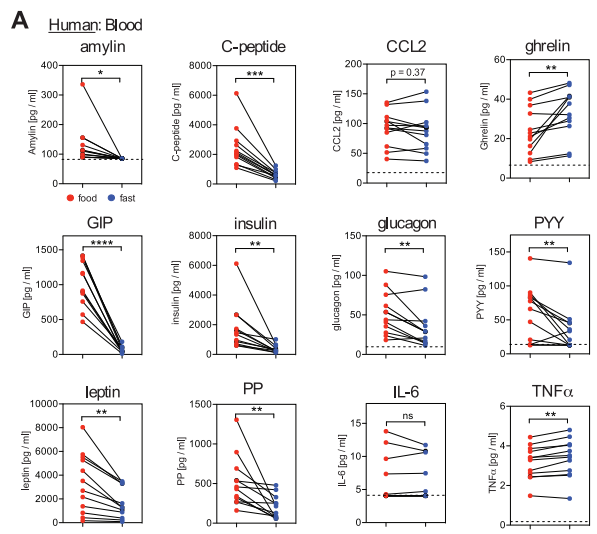


Figure S4. PPAR α Controls Steady-state Blood and Tissue CCL2 Levels. Related to Figure 4

(A) Multiplex analysis for metabolic hormones in healthy humans. Dots represent paired analysis of individual samples. Dotted lines = limit of detection.

(B) Absolute numbers of Ly-6C^{high} monocytes in fasting wt and *Ccr2*^{-/-} mice that were gavaged with glucose for 4 hr.

(C) Levels of CCL2 protein in indicated tissues.

(D) Level of CCL2 protein in bone marrow extracellular fluid (BMEF) in mice that were fed or fasted for 4 hr.

(E) *Alb*^{cre/cre} mice were crossed to *Ccl2*^{fl/fl} mice to delete *Ccl2* from hepatocytes (*Ccl2* ^{Δ Hep}). CCL2 levels and absolute numbers of Ly-6C^{high} monocytes in the blood of cre+ mice deficient in liver CCL2 or cre- littermate controls are shown.

(F) CCL2 levels and absolute numbers of Ly-6C^{high} monocytes in the blood of splenectomized mice.

(G) Representative immunofluorescence of bone marrow sections stained for CCL2 (green) and nuclei (DAPI, blue). Insert zooms in on CCL2 positive cells. Scale bar 10 μ m.

(H) Plot shows CCL2 production in BM versus CCL2 levels in plasma.

(I) Significantly changing serum proteins were mapped on differentially expressed genes in hepatocytes upon fasting.

(B to F, H) Every dot represents one individual animal. Horizontal bar = mean. Vertical bar = SD. Student's t test was performed (A, B, D to F). Statistical significance is indicated by *p < 0.05, **p < 0.01, ***p < 0.001, ****p < 0.0001. ns = not significant.

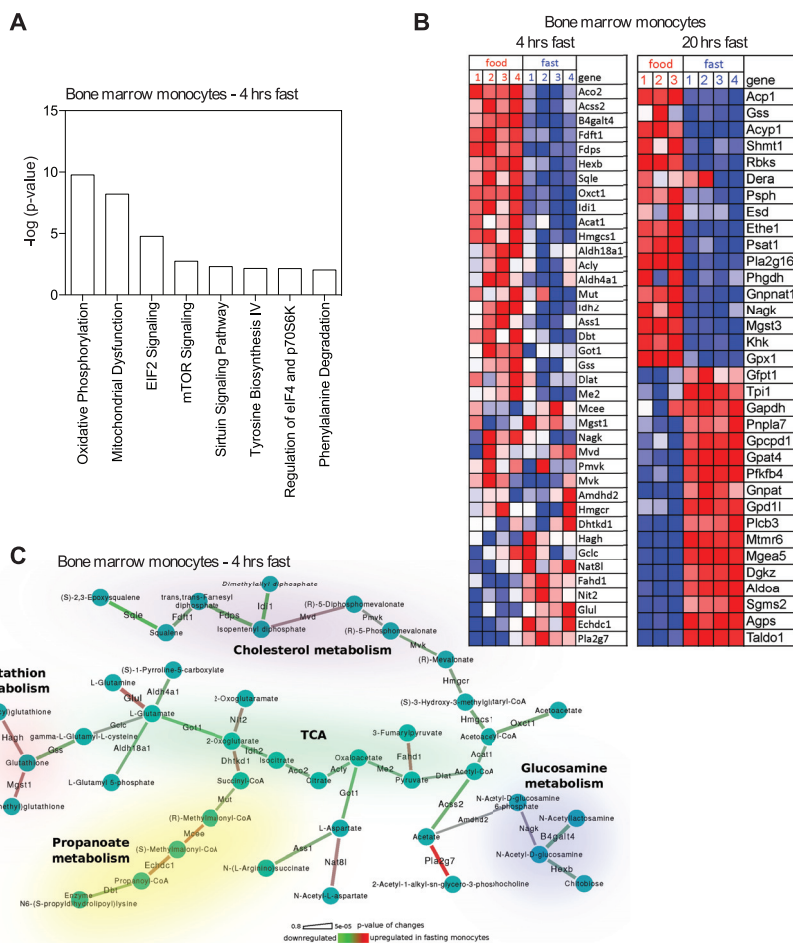


Figure S5. Fasting Modifies Monocyte Metabolic Activity. Related to Figure 5

(A) Ingenuity Pathway Analysis (IPA) of differentially expressed genes in monocytes between mice that were fed or fasted for 4 hr.

(B and C) Integrated metabolic network analysis of the transcriptional differences in monocytes from mice that were fed or fasted for 4 hr or 20 hr. (B) Heatmaps show scores for subnetwork metabolic enzymes. (C) Graphical representation of the regulated metabolic subnetwork in mice that were fed or fasted for 4 hr.

Figure S6. Fasting Improves Inflammatory Disease Outcome. Related to Figure 6

(A, B, C) Differentially expressed genes in bone marrow monocytes from mice that were fed or fasted for 20 hr were analyzed using Ingenuity Pathway Analysis (IPA). Heatmaps show z-scores of genes related to the indicated gene sets.

(D) EAE clinical course in wild-type controls and *Ccr2*^{-/-} mice.

(E, F, G, H) Mice were fed *ad libitum* (AL) or subjected to intermittent fasting in 24 hr cycles (IF) for 4 weeks before EAE induction and during disease development. Numbers of (E) Ly-6C^{high} monocytes, (F) neutrophils and (G) T cells in the blood are shown. (H) Monocytes were purified from spinal cords and transcriptionally profiled at day 21 post EAE induction. Heatmaps display z-scores of genes related to the indicated gene sets.

(I, J) Mice were fed *ad libitum* or fasted for 20 hr prior to infection with *L. monocytogenes*. (I) Absolute numbers of Ly-6C^{high} monocytes in the blood and the bone marrow. (J) *L. monocytogenes* colony-forming units (CFU) in the spleen.

(K, L, M) Mice were fed *ad libitum* (AL) or subjected to intermittent fasting in 24 hr cycles (IF) for 6 weeks prior to infection with *L. monocytogenes*. (K) Graph shows CCL2 levels in blood. (L) Absolute numbers of T cells in blood and (M) spleen are shown.

(N) Wound healing kinetics in mice that were fed or fasted for 20 hr prior to wounding.

(O, P, Q) Mice were fed *ad libitum* (AL) or starved for 48 hr (ST) prior to infection with *L. monocytogenes*. (O) Absolute numbers of Ly-6C^{high} monocytes in the blood, bone marrow and spleen are shown. (P) Graph shows CCL2 levels in blood. (Q) *L. monocytogenes* colony-forming units (CFU) in the spleen.

(R) Wound healing kinetics in mice that were fed *ad libitum* (AL) or starved for 48 hr (ST) prior to wounding.

(E-G, I-M, O-Q) Every dot represents one individual animal. Horizontal bar = mean. Vertical bar = SD. Two-way analysis of variance (ANOVA) (D, N, R) or One-way ANOVA with Bonferroni's post test (I, K, L, M, O, P) or Student's t test (E, F, G, J, Q) were performed. Statistical significance is indicated by *p < 0.05, **p < 0.01, ***p < 0.001, ****p < 0.0001. ns = not significant.